Combining collective, MSW, and turbulence effects in supernova neutrino flavor evolution

Tina Lund and James P. Kneller

Phys. Rev. D **88**, 023008 — Published 16 July 2013

DOI: 10.1103/PhysRevD.88.023008

Combining collective, MSW, and turbulence effects in supernova neutrino flavor evolution

Tina Lund[1] and James P. Kneller[1]

[1] *Department of Physics, North Carolina State University, 2401 Stinson Drive, Raleigh, USA*

(Dated: June 11, 2013)

In order to decode the neutrino burst signal from a Galactic core-collapse supernova (ccSN) and reveal the complicated inner workings of the explosion we need a thorough understanding of the neutrino flavor evolution from the proto-neutron star outwards. The flavor content of the signal evolves due to both neutrino collective effects and matter effects which can lead to a highly interesting interplay and distinctive spectral features. In this paper we investigate the supernova neutrino flavor evolution in three different progenitors and include collective flavor effects, the evolution of the Mikheyev, Smirnov & Wolfenstein (MSW) conversion due to the shock wave passage through the star, and the impact of turbulence. We consider both normal and inverted neutrino mass hierarchies and a value of θ_{13} close to the current experimental measurements. In the Oxygen-Neon-Magnesium (ONeMg) supernova we find that the impact of turbulence is both brief and slight during a window of 1–2 seconds post bounce. This is because the shock races through the star extremely quickly and the turbulence amplitude is expected to be small, less than 10%, since these stars do not require multi-dimensional physics to explode. Thus the spectral features of collective and shock effects in the neutrino signals from Oxygen-Neon-Magnesium supernovae may be almost turbulence free making them the easiest to interpret. For the more massive progenitors we again find that small amplitude turbulence, up to 10%, leads to a minimal modification of the signal, and the emerging neutrino spectra retain both collective and MSW features. However, when larger amounts of turbulence is added, 30% and 50%, which is justified by the requirement of multi-dimensional physics in order to make these stars explode, the features of collective and shock wave effects in the high (H) density resonance channel are almost completely obscured at late times. Yet at the same time we find the other mixing channels - the low (L) density resonance channel and the non-resonant channels - begin to develop turbulence signatures. Large amplitude turbulent motions in the outer layers of more massive, iron core-collapse supernovae may obscure the most obvious fingerprints of collective and shock wave effects in the neutrino signal but cannot remove them completely, and additionally bring about new features in the signal.

PACS numbers: 97.60.Bw, 14.60.Pq

I. INTRODUCTION

Our understanding of how massive stars explode continues to evolve at a frenetic pace due to advances in the hydrodynamical modelling [1–23]. The long-sought goal of simulating successful explosions based upon first-principle physics appears to be imminent, and emerging from that is a basic paradigm with the collapse of the core followed by the formation of a shock which propagates out to $r \sim 200$ km before stalling. Due to a mixture of neutrino heating and/or the Standing Accretion Shock Instability (SASI) [1–9] the outward motion of the shock is revived after a delay of up to $t \sim 500$ ms. The shock then makes its way through the mantle of the star to eventually reach the surface creating the spectacular fireworks we observe.

As impressive as the optical emission from core-collapse supernovae (ccSNe) may be, the neutrino burst from the next ccSN in our Galaxy will outshine the rest of the Universe in neutrinos and represents an unparalleled opportunity to learn about the dynamics at the core of the explosion. The potential of the signal to answer outstanding questions in physics and astrophysics was recently reviewed by Scholberg [24]. For example, the neutrino emission during the accretion phase leaves telltale oscillatory features which may be observed in large water/ice Cerenkov detectors such as IceCube as shown by Lund *et al.* [25, 26], and from the IceCube event rate the hierarchy might be inferred [27]. Decoding the neutrino burst signal will not be easy, however, because our detectors are sensitive to the neutrino flavor, and the flavor content of the signal is a function of both time, energy and emission point from the proto-neutron star. As the neutrinos propagate through the supernova mantle two time dependent flavor transformation processes can occur: collective (self-interaction) effects during the first ~ 1000 km or so, and the Mikheyev, Smirnov & Wolfenstein (MSW) [28, 29] effect which occurs when the matter density is in the range of $1\ \mathrm{g/cm^3} \leq \rho \leq 10^4\ \mathrm{g/cm^3}$ for neutrino energies of order $1 - 100$ MeV.

Neutrino collective effects are a very active field of study with significant and ongoing progress. Initially investigations were primarily in terms of effective two flavor calculations (see e.g. [30–40]) but lately more and more investigations consider three flavors (see e.g. [41–49]). The phenomenology of collective effects with three flavors has been found to be much richer than for two with new effects appearing such as multiple splits for both neutrinos and anti-neutrinos in either hierarchy (e.g. Dasgupta *et al.* [45]). Over time it has also been realized

that the standard set of luminosity and energy values employed (equipartition of luminosities and a strong hierarchy of energies) is a special case rather than being a generalizable choice of values. In calculations of collective effects typical values used for the mean energies are $E_{\nu_e} = 10 - 12$ MeV, $E_{\bar{\nu}_e} = 15 - 16$ MeV and $E_{\nu_x} = 16 - 27$ MeV [31, 33, 45, 50] along with equipartition of the luminosities. Smaller energy differences are found in recent long term simulations, e.g. Hüdepohl *et al.* [14] and Nakazato *et al.* [13], where energies are on the order of $E_{\nu_e} = 9 - 10.1$ MeV, $E_{\bar{\nu}_e} = 11.5 - 12.9$ MeV and $E_{\nu_x} \sim 13$ MeV. Among others, Roberts *et al.* [51] and Horowitz *et al* [52] have pointed out that the neutrino opacities and interaction cross sections used by the modeling community are not as correct as they could be. Previous statements by Reddy *et al.* [53] along the same lines lead to recalculations by Martínez-Pinedo *et al.* [54] of some of the simulations from [11], although not to post bounce times as late as those available from Fischer *et al.* [11]. The findings of Martínez-Pinedo *et al.* [54] indicate that the inclusion of the correct opacities will lead to an overall lowering of the luminosities, and a reduction, respectively increase, of the ν_e and $\bar{\nu}_e$ energies. A similar conclusion was reached by Horowitz *et al.* [52] in their short duration 1D simulations. As a result of the ongoing improvements to the simulations the energy and luminosity values are continously adjusted. Investigations have scanned parts of the parameter space of luminosities and energies (e.g. Fogli *et al.* [32]) but they have not been exhaustive. Even more recently it has been found there are new flavor instabilities due to flavor dependent angular distributions at the neutrinosphere [41], and possibly an additional effect, known as the neutrino halo, due to the scattering of the neutrinos [43, 49, 55].

At the present time the understanding of the neutrino self-interaction is not sufficient to be able to predict results except in the broadest sense. The linear stability analysis of Banerjee *et al.* [56] and Sarikas *et al.* [57, 58], extended in Mirizzi & Serpico [41, 42] and Saviano *et al.* [59] allows one to analyze the system and demonstrate the existence of the conditions that lead to the collective phenomena but not the details. The non-linear nature of the neutrino self-interaction and the strong dependence that has been discovered on even small differences in L and E means we do not yet possess the analytical predictive power over the resulting features and their behavior. We therefore have to primarily rely on numerical calculations to expand our knowledge.

The flavor transformation due to the MSW effect is also non-trivial because the passage of the shock wave through the star leaves an impression in the signal [50, 60–65]. A further complication is the possible presence of density fluctuations/turbulence [30, 66–71] which one would expect to be created by the large scale inhomogeneities generated during the accretion phase. A turbulent density profile would also imply neutrinos of the same energy arriving at the same time in a detector but emitted from different locations at the proto-neutron star will not have experienced the same flavor density profile history [72, 73]. Finally, once the star is left behind and the neutrinos have reached Earth recent studies indicate that fortunately/unfortunately (depending upon one's point of view) Earth matter effects on the neutrino signal may be minimal [74].

For the most part the various neutrino flavor transformation processes have been studied in isolation, see Gava *et al.* [65] for an exception, but of course the neutrino signal is the denouement involving all these protagonists. In order to understand the explosion narrative we must determine which process left which features in the signal and how they interacted. The aim of this paper is to study the interplay of the various neutrino flavor transformation processes that can occur in core-collapse supernovae by exploring the features each engenders separately and in combination. For our calculations we use the density profiles and neutrino spectra from the hydrodynamical simulations by Fischer *et al.* [11], consider both normal and inverted hierarchies and use a value of θ_{13} close to the recent experimental results from T2K [75], Double Chooz [76], RENO [77] and Daya Bay [78].

The organization of this paper is as follows. In order to assist the reader we first describe in Sec. II the similarities and differences between the density profiles, and the neutrino spectra from the three simulations pointing out important features relevant for the neutrino flavor evolution. We then describe the evolution calculations and how we modified the profiles to steepen the shocks and insert turbulence. In Sec. III we walk the reader through the different signatures inserted into the signal by each transformation process at a given snapshot during the explosion. Then we run through how these features evolve with time in Sec. IV. We present our conclusions in section Sec. V.

II. DESCRIPTION OF THE CALCULATIONS

A. Theory and background

In order to construct the neutrino burst signals here at Earth there are many calculated components one needs to put together. Our first task is to calculate the probability that a neutrino in a particular initial state emerges from the supernova in a given final state. These probabilities depend upon the basis and for supernova neutrinos the most useful transition probabilities are those linking the initial flavor state ν_α to the mass eigenstate ν_i. The mass eigenstates are the states which diagonalize the vacuum Hamiltonian and the reason we need the probability of emerging in these states - and not the probability that the neutrino emerges in a flavor state - is because the neutrino wave packet will decohere on its passage to Earth and will arrive as separate mass states. This probability, $P_{i\alpha} = P(\nu_\alpha \to \nu_i)$, can be found quite easily from the S-matrix linking the initial neutrino flavor states to the final mass states i.e. $P_{i\alpha} = |S_{i\alpha}|^2$. In this paper we

TABLE I. Characteristics of our 3 numerical models. All times are post bounce. Further details can be found in [11].

Model	8.8 $M_\odot$	10.8 $M_\odot$	18.0 $M_\odot$
Simulation end time [s]	4.541	10.545	21.804
Shock revival time [ms]	~ 30	$\simeq 300$	$\simeq 300$
EoS	Shen	Shen	Shen
Progenitor from	Nomoto (83, 84 & 87)	Woosley *et al.* (02)	Woosley *et al.* (02)

shall use $\bar{P}_{i\alpha}$ for the anti-neutrino probabilities and the symbol $\bar{S}$ for the anti-neutrino S-matrix. There is a third basis one often sees in the literature known as the matter basis [47, 79]. This basis is the most useful one for actually doing the calculations plus the matter basis states closely align with the flavor states at the neutrinosphere and the mass states in the vacuum. Throughout this paper we will show results in the matter basis transition probabilities and we refer the reader to [47, 79] for the definition of this basis and its detailed connection with the other two bases. Briefly put the matter basis is related to the flavor basis by the usual mixing matrix, but with the the mixing angles modified.

The S-matrix is found by solving the Schrödinger equation

$$\imath \frac{dS}{dx} = HS \tag{1}$$

where H is the Hamiltonian. For neutrino propagation in supernova the Hamiltonian is composed of three parts: the vacuum H_V, the MSW contribution H_{MSW} and the neutrino self-interaction $H_{\nu\nu}$.

The vacuum Hamiltonian H_V in the mass basis is diagonal and parameterized by two mass squared differences $\delta m^2_{ij} = m^2_i - m^2_j$ and the neutrino energy E. The vacuum Hamiltonian in the flavor basis is related to the mass basis by the Maki-Nakagawa-Sakata-Pontecorvo [80, 81] unitary matrix parameterized by the three mixing angles, θ_{12}, θ_{13} and θ_{23}, a CP phase and two Majorana phases. The Majorana phases have no effect upon the evolution [47, 82] and will be ignored. In our calculations we will employ the following values for the mass splittings and mixing angles: $\theta_{12} = 34.4°$, $\theta_{13} = 9°$, $\theta_{23} = 45°$, $\delta m^2_{21} = 7.59 \times 10^{-5}$ eV^2 and $\delta m^2_{32} = 2.43 \times 10^{-3}$ eV^2, and we take δ, the CP-violating phase, to be zero.

B. The MSW potential and the density profiles

The MSW potential describes the effect of the background matter upon the neutrino and this contribution is diagonal in the flavor basis. In this paper we shall only consider the effect of matter upon the electron neutrino and anti-neutrino and ignore the small $\mu\tau$ potential which, in the standard model, is a factor of $\sim 10^{-5}$ smaller. Consequently only the e, e component of H_{MSW} is non-zero and is equal to $\sqrt{2} G_F n_e(\mathbf{r})$ where G_F is the Fermi constant and $n_e(\mathbf{r})$ the electron density. The effect of matter upon the anti-neutrinos is opposite that of the neutrinos i.e. $\bar{H}_{MSW} = -H_{MSW}$. The electron density is calculated from matter density profiles generated by the Basel simulation group [11]. A thorough explanation of the simulations can be found in [11]. We therefore refrain from going into details about them here, and merely give the most basic information on each progenitor in Table I.

The density profiles come from three one-dimensional numerical simulations of progenitors with masses of 8.8 $M_\odot$, 10.8 $M_\odot$ and 18.0 $M_\odot$. The simulations ran to a post bounce (pb) time of 4.5 s, 10.5 s and 21.8 s respectively. Not every snapshot from the simulations are used. We sample the profiles at 1 second intervals after bounce for a total of 5, 11 and 11 profiles for the 8.8 $M_\odot$, 10.8 $M_\odot$ and the 18.0 $M_\odot$ model respectively (see Table II).

In Fig. 1 we show the 6 density profiles that will be the main focus of this paper. The top panel shows the 1 second profiles for all three progenitors; a solid black line for the 8.8 $M_\odot$ progenitor, a dashed red line for the 10.8 $M_\odot$ model and in dot-dashed blue the 18.0 $M_\odot$ model. The bottom panel similarly shows the density profiles at 3 s pb, which is well into the cooling phase. In the profiles for the 18.0 $M_\odot$ model (blue dot-dashed lines) a forward shock is present at both 1 and 3 seconds. The same is

TABLE II. Post bounce times for the investigated density profiles of our three progenitor models.

Post bounce time [s]	8.8 $M_\odot$	10.8 $M_\odot$	18.0 $M_\odot$
Bounce	0.000	0.000	0.000
1	1.006	0.815	0.980
2	2.006	1.814	1.982
3	3.005	2.816	3.007
4	3.992	3.811	4.005
Last	4.491		
5		4.829	5.000
6		5.809	5.979
7		6.807	7.024
8		7.813	7.996
9		8.814	8.996
10		9.815	9.985
Last		10.545	10.985

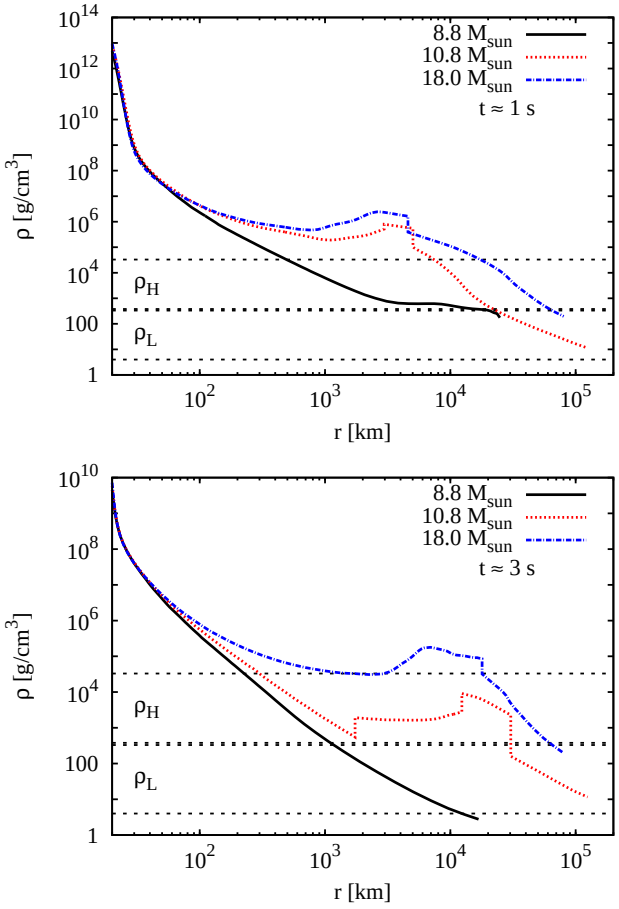

FIG. 1. (color online). Density profiles at ∼1 s (*top*) and ∼3 s (*bottom*) for our three progenitor models: 8.8 $M_\odot$ (black solid line), 10.8 $M_\odot$ (red dashed line) and 18.0 $M_\odot$ (blue dot-dashed line). The horizontal gray dashed lines encompass the MSW resonant densities for neutrinos with energies in the range 1–100 MeV. The upper band corresponds to the H resonance and the lower band to the L resonance.

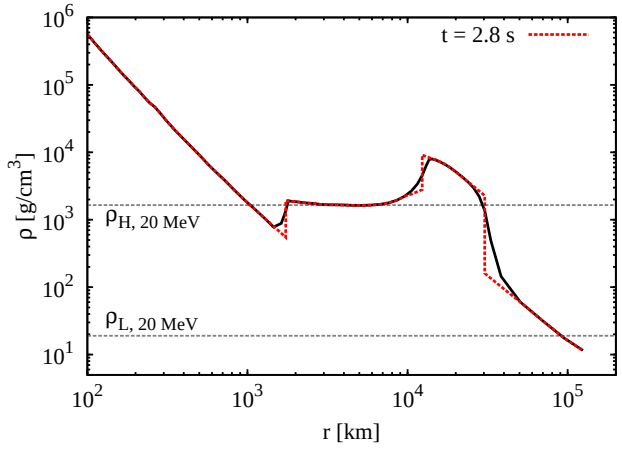

FIG. 2. (color online). Initial density profile (black solid line) and steepened version (red dashed). The profile is from the 10.8 $M_\odot$ model at 2.8 s. The horizontal gray dashed lines give the resonant densities for a 20 MeV (anti)neutrino in the H and L density regions.

the case with the 10.8 $M_\odot$ model (the forward shock is at $\sim$ 5000 km at 1 s and at $\sim$ 30.000 km at 3 s (red dashed lines)). Here additionally though, the contact discontinuity has developed both at 1 and 3 s (seen as the abrupt change in density around $\sim$ 3000 km in the upper panel of Fig. 1). The contact discontinuity arises at the interface of the dense ejecta shell just below the forward shock and the less dense ejecta region below it which is heated by neutrinos [83]. In the 3 second profile of the 10.8 $M_\odot$ progenitor (lower panel of Fig. 1) also the reverse shock has materialized, which is identified as the abrupt change in density at $\sim$ 1700 km. The reverse shock develops when the low density, neutrino heated outflow (the neutrino-driven wind) is accelerated to supersonic velocities and crashes into the denser, slower moving, shock accelerated ejecta ahead of it. The wind is quickly decelerated thereby forming the reverse shock [11]. Subsequently the reverse shock continues to move outward with a speed similar to, or sligthly slower than, that of the forward shock. In Fig. 4 the placement of the density features in the 2.8 s profile of the 10.8 $M_\odot$ progenitor has been marked. Neither the contact discontinuity nor the reverse shock are present in the 8.8 $M_\odot$ model profiles at the times we use.

We have had to modify slightly the profiles plotted in Fig. 1. The original density profiles did not have sufficiently steep shocks, which is a known complication due to insufficient radial resolution in numerical simulations. We therefore steepened by hand both shocks and the contact discontinuity into actual discontinuous jumps. In Fig. 2 we show an original density profile (solid black line) and the steepened version of the same profile (red dashed line).

To illustrate precisely how crucial the steepness of the density profile is with the currently favored large value of θ_{13}, we show in Fig. 3 the matter state probabilities for the original density profile at 2.8 s for the 10.8 $M_\odot$ progenitor and for the steepened version. The probabilities are for a calculation with a 20 MeV (anti-)neutrino propagating from the PNS surface to the end of the density profile without turbulence. We clearly see with the profile that was not steepened (left quartet) that nothing happens to the probabilities as the neutrino pass the shocks or the contact discontinuity because all of them are too adiabatic. On the other hand as the neutrino traverses the steepened profile (right quartet) we see how the diabatic passage at the shocks and the contact discontinuity leads to mixing of the neutrino states. In the left quartet we see that the divergence from unit survival probability has begun before we reach the radius of the reverse shock, and it can therefore be attributed to collective effects. As the neutrino passes through features in the density profile nothing new happens in the probabilities. In the right quartet we see the same small divergence from unit survival probability at low r values, and once

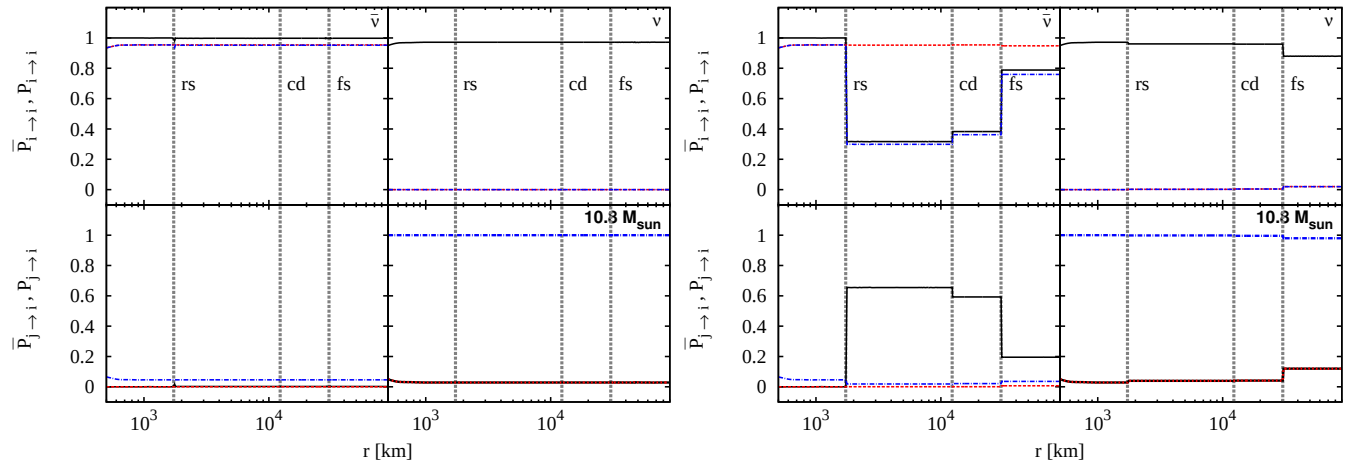

FIG. 3. (color online). Matter state survival and transition probabilities for $\bar{\nu}$ (*left* panels of each quartet, $\bar{P}$) and ν (*right* panels of each quartet, P) for a calculation from the PNS surface to the end of the density profile at 2.8 s pb from the 10.8 $M_\odot$ model. Matter survival probabilities $P_{\nu_i \to \nu_i}$ are shown in the upper panels of each quartet, and transition probabilities $P_{\nu_i \to \nu_j}$ are shown in the bottom ones. The solid black lines indicate the probabilities for ending in matter state 1 (or anti-matter state $\bar{1}$ in the case of anti-neutrinos), the red dashed lines give the probabilities of ending in matter state 2 ($\bar{2}$) and finally the blue dot-dashed lines give the probabilities for ending in matter state 3 ($\bar{3}$) at the end of the calculation domain. See the text for more explanation. The left quartets correspond to the original density profile, the right quartets to the steepened density profile, both in the IH. The vertical gray dashed lines mark the positions of the reverse shock (rs), the contact discontinuity (cd) and the forward shock (fs).

again this is caused by the collective neutrino interaction (this will be demonstrated further in Sect. III A). As the radius of the reverse shock is reached we see as expected in the IH the enhanced mixing of anti-neutrino states $\bar{1}$ and $\bar{3}$ caused by the MSW H resonance. Consequently the survival probability of states $\bar{1}$ (black solid line) and $\bar{3}$ (dot-dashed blue line) drops from unity as they are converted into each other. When the forward shock is traversed the resonant enhancement reverts the previous mixing and the survival probability returns to almost unity. At the forward shock we also observe a decrease in the survival probability of the neutrino state 1, which is caused by the MSW L resonance (This will be discussed further in Sect. IV.)

With the plethora of differences between the survival probabilities of the steepened and the un-steepend density profiles correct calculations of the neutrino flavor evolution obviously requires steep density profiles to ensure the diabatic resonance crossing we know should take place.

C. Turbulence

The turbulence we include in the calculations will enter through the MSW potential. Our approach follows that of [64, 69] and many others whereby we multiply the smooth, turbulence free, density profiles from the one-dimensional hydrodynamical supernova simulations, which we call $\langle n_e \rangle$, with a Gaussian random field $1+F(r)$. The turbulence is placed into the three models slightly differently. For the 10.8 $M_\odot$ model we place one turbulence field between the forward shock and contact discontinuity and then another between the contact discontinuity and the reverse shock if the reverse shock is present. For the 18.0 $M_\odot$ model we let one turbulence field cover the entire region behind the forward shock since neither a contact discontinuity nor a reverse shock develops in this model. Finally, for the 8.8 $M_\odot$ model we again insert the turbulence behind the shock but the shock in this model quickly runs out of the simulation domain and thereafter we allow the turbulence to cover all of the profile. At no point is turbulence placed into the profile ahead of the forward shock. The amplitudes of the turbulence seen in the simulations by Meakin & Arnett [84] are very small, typically between $\sim 10^{-5}$ to $\sim 10^{-3}$, and we have verified that this is too small to affect the neutrinos.

The Gaussian field is modelled as a Fourier series with a normalized power spectrum $E(k)$ multiplied by two damping factors to suppress fluctuations close to the shocks and contact discontinuity and prevent discontinuities. Concretely, we use

$$F(r) = C_\star \tanh\left(\frac{r - r_r}{\lambda}\right) \tanh\left(\frac{r_s - r}{\lambda}\right) \times \sum_{n=1}^{N_k} \sqrt{V_n}\left\{A_n \cos\left(k_n\, r\right) + B_n \sin\left(k_n r\right)\right\}. \quad (2)$$

for radii between $r_r \le r \le r_s$ and zero outside this range. The damping scale λ is set to $\lambda = 100$ km and the parameter $C_\star$ sets the amplitude. Each of the N_k co-efficients in the sets $\{A\}$ and $\{B\}$ are independent standard Gaussian random variates with zero mean thus ensuring a vanishing expectation value of F. Finally, the parameters V_n

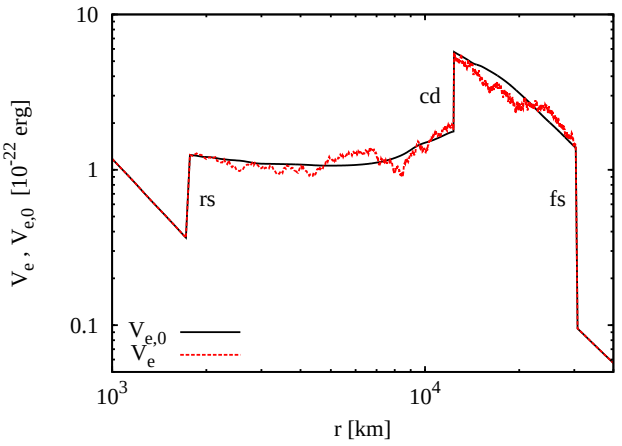

FIG. 4. (color online). Close up of the unperturbed potential $V_{e,0}$ (black solid line) at 2.8 s for our 10.8 $M_\odot$ model and the potential with turbulence added, V_e (red dashed line). The two areas with added turbulence are: between the forward shock (fs) and the contact discontinuity (cd), and between the contact discontinuity and the reverse shock (rs).

are k-space volume co-efficients. To generate the N_k k's, V's, A's and B's for a realization of F we use 'Variant C' of the Randomization Method the reader can find in Kramer, Kurbanmuradov, & Sabelfeld [85]. The algorithm behind this randomization method is to partition k-space into N_k regions and from each select a random wavenumber using the power-spectrum, $E(k)$, as a probability distribution. The volume parameters V_n are the integrals of the power spectrum for each partition. Variant C of the Randomization Method divides the k-space so that the number of partitions per decade is uniform over N_d decades starting from a cutoff scale $k_\star$. We shall use a wavenumber cutoff $k_\star$ set to $k_\star = \pi/\Delta r$. Where Δr is the distance between the discontinuities under consideration. This logarithmic distribution of the modes is designed so that the quality of the realizations is uniform over the range of length scales considered, i.e. it is scale invariant. This feature is important because the oscillation wavelength of the neutrinos is constantly changing as the density evolves. All the results in this paper shall adopt $N_d = 4$ and $N_k = 40$ but to reassure the reader we have checked several of our results with the combination $N_d = 5$ and $N_k = 50$.

In Fig. 4 we show an example from the 10.8 $M_\odot$ model where 10% turbulence has been added to the potential at 2.8 s pb. The unperturbed potential $V_{e,0}$ is shown in solid black and the turbulent potential V_e is shown in red dashed. We have furthermore marked the reverse shock (rs), the forward shock (fs) and the contact discontinuity (cd), which are all present in this particular profile.

D. Neutrino self-interactions

Finally, the neutrino density in the innermost regions of the supernova is so high that neutrinos become a background to themselves leading to a non-linear self-coupling. The extended source of the neutrinos means that at some given radial position r above the neutrinosphere one will find neutrinos propagating in a wide swath of directions relative to the radial direction. In principle the evolution of each has to be calculated simultaneously but often the reader will observe the use of the single angle approximation which treats all outward directions as being equivalent. At the present time the validity of the single-angle approximation is unclear. Duan & Friedland [46] compared single angle and "multi-angle" calculations and observed a rapid onset of neutrino transformation due to collective effects in their single angle calculations that did not occur in multi-angle calculations. At the same time it was shown in [58] that single angle calculations can match multi-angle calculations. It is not our intention to wade into this debate here. We shall adopt the single angle approximation because it makes the numerous calculations we must undertake feasible and its results are "realistic" in the sense that they give the same (or similar) features as the multi-angle calculations. Through private communication, we have learned that our results for the collective effects match quantitatively the results found by Lunardini & Tamborra, who performed multi-angle calculations on some of the time snapshots from the Basel progenitors in their recent paper [86].

The single-angle self-interaction Hamiltonian in the flavor basis is of the form

$$H_{\nu\nu} = \frac{\sqrt{2}\,G_F}{2\,\pi\,R_\nu^2}\,C(r/R_\nu)\,\left\{\int dE_\nu S(r,E_\nu)\rho(r_0,E_\nu)S^\dagger(r,E_\nu) - \int dE_{\bar\nu}\left(\bar S(r,E_{\bar\nu})\bar\rho(r_0,E_{\bar\nu})\bar S^\dagger(r,E_{\bar\nu})\right)^\star\right\} \qquad (3)$$

where $\rho(r_0,E_\nu)$ is the energy dependent density matrix for the neutrinos at the initial point r_0 and similarly $\bar\rho(r_0,E_{\bar\nu})$ is for the anti-neutrinos. We shall adopt $r_0 = 70$ km and we have verified that our results do not depend upon the initial starting radius. The radius of the neutrinosphere is R_ν and the function $C(r)$ is commonly known as the geometric factor. For this paper we shall adopt the form given in [87]

$$C(r) = 4\,\frac{R_\nu^2}{r^2}\,\left[\frac{1-\sqrt{1-R_\nu^2/r^2}}{R_\nu^2/r^2}\right]^2 - \frac{R_\nu^2}{r^2}\quad .$$

The neutrino spectral information is buried inside the two density matrices $\rho(r_0,E_\nu)$ and $\bar\rho(r_0,E_{\bar\nu})$. To model

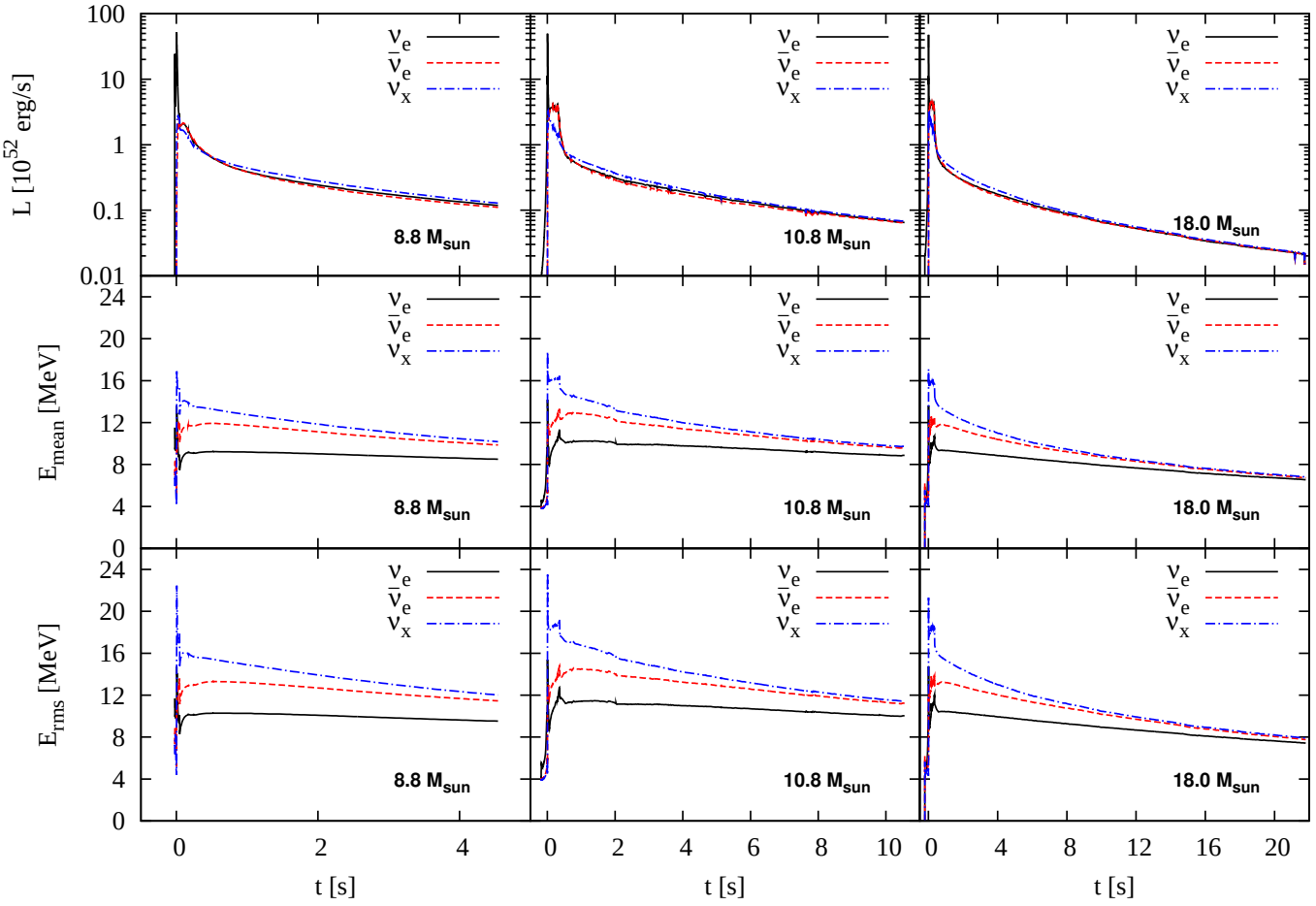

FIG. 5. (color online). Luminosity (*top*), mean energy (*middle*) and rms energy (*bottom*) for the three models; 8.8 $M_\odot$ (*left*), 10.8 $M_\odot$ (*middle*) and 18.0 $M_\odot$ (*right*). Black solid lines designate electron neutrinos ν_e. Red dashed lines show electron anti-neutrinos $\bar{\nu}_e$. Blue dot-dashed lines show non-electron flavor neutrinos ν_x. The non-electron anti-neutrino, $\bar{\nu}_x$, quantities are almost identical to the ones of their neutrino counterparts.

the neutrino spectra we use the 'pinched' spectra found in Keil *et al.* [88], and the luminosities and mean energies supplied from the Basel group [89]. The pinch parameters are computed from the ratio of rms to mean energy. Luminosities and energies are shown in Fig. 5. During the accretion phase (up to ~ 0.5 s) the electron neutrino luminosities, L_{ν_e}, dominates, but during the cooling phase the non-electron neutrino luminosities, L_{ν_x}, are largest. At very late times all luminosities become very similar. The mean energies show a distinct hierarchy at early times, $E_{\nu_x,\bar{\nu}_x} > E_{\bar{\nu}_e} > E_{\nu_e}$, while at later times the $E_{\bar{\nu}_e}$ and $E_{\nu_x,\bar{\nu}_x}$ become much more similar and their dominance over E_{ν_e} becomes smaller.

As we mentioned in the introduction, the accuracy of simulations is continously improving, particularly with respect to the neutrino opacities. We acknowledge these improvements in more recent simulations but we find that the disagreement on the exact size and impact is still large, and that the difference due to including the updated cross sections or not is on the order of changing the equation of state of the progenitor, as can be seen from O'Connor & Ott [23]. Furthermore, using luminosities, energies and density profiles from the same simulation allows us to carry out our calculations selfconsistently. Therefore we will use the older simulations [11] covering the longer post bounce times.

III. RESULTS

In order to pick apart a neutrino burst signal and be confident we have identified features caused by the neutrino self-interactions from those generated by the MSW effect or the turbulence we must first understand the features each engenders separately before seeing how they combine. But with so many simulation snapshots, three different progenitors and two hierarchies we find a virtual zoo of phenomena. In order for the reader to understand our later results we begin by walking through our results for a single case. To keep things simple we chose the profiles of each simulation at 3 seconds post bounce when the shock has propagated far enough into the star that it

begins to affect the MSW resonance. We then undertake four different calculations for this simulation snapshot of each model:

- an 'inner region' calculation from the proto-neutron star up to 1000 km where the collective effects are expected to be dominant.
- an 'outer region' calculation that covers from 1000 km to the end of the profiles where the MSW effect dominate the flavor evolution.
- a 'turbulence free' calculation which covers the entire profile but with no added turbulence,
- a 'turbulent' calculation which again covers the entire profile but now various amounts of turbulence is added according to the prescription given previously.

A. Profiles at 3 seconds

1. *Inner region, 70 – 1000 km: Collective dominated*

The results of our calculations for inner region, where collective effects dominate, for the simulation snapshot at 3 s pb are shown in Fig. 6 for the Inverted Hierarchy (IH) and in Fig. 7 for the Normal Hierarchy (NH). In each figure the top four panels are for the 8.8 $M_\odot$ progenitor, the middle four panels are for the 10.8 $M_\odot$ progenitor and the bottom four panels are for the 18.0 $M_\odot$ progenitor. Then, within each quartet of panels, the left two panels show the probabilities for the anti-neutrino matter states and the right two panels show the neutrino matter state probabilities. The top two panels of a quartet show the survival probabilities ($P_{\nu_i \to \nu_i}$), and the bottom two show selected transition probabilities ($P_{\nu_i \to \nu_j}$). The remaining transition probabilities can be found from probability conservation. In the top right (left) panels of each quartet the solid black line gives the probability that neutrino (anti-neutrino) matter state 1 ($\bar{1}$) goes to matter state 1 ($\bar{1}$). In the lower right (left) panels of each quartet the black line signifies the probability that neutrino (anti-neutrino) matter state 3 ($\bar{3}$) goes to matter state 1 ($\bar{1}$). Similarly the red dashed line in the top panels are matter state 2 ($\bar{2}$) to 2 ($\bar{2}$), and the blue dot-dashed line is matter state 3 ($\bar{3}$) going to 3 ($\bar{3}$). In the lower panels the red dashed line indicates matter state 1 ($\bar{1}$) going to matter state 2 ($\bar{2}$), and the blue dot-dashed line represents matter state 2 ($\bar{2}$) going to matter state 3 ($\bar{3}$). The legend is the same for each quartet in subsequent figures in this paper which is why it only appears in the top left quartet of each pair of figures.

From Figures 6 and 7 we see that in both hierarchies all three models have at least two spectral splits (also known as 'swaps') in the neutrino sector. Spectral splits are sudden changes in the transition probabilities as a function of neutrino or anti-neutrino energy and have been observed in self-interaction calculations starting from Duan *et al.* [33]. Sets of complete and incomplete swaps[1] between the neutrino states are very typical of all self-interaction calculations and the results depend upon the hierarchy. In the IH (Fig. 6) the splits are between neutrino matter states 2 and 3 occurring at 7–8 MeV and 24–28 MeV depending on the progenitor. From the top right panels of each quartet we see that between these two energies the survival probabilities of the two states drop to zero. Looking in the bottom right panels of each quartet we learn that in this energy range the matter state 2 goes to matter state 3, and that 3 does not go (significantly) to state 1, thus it must transform into matter state 2. Therefore, we conclude that a full swap of matter states 2 and 3 takes place between the two swap energies in the spectrum. In the NH (Fig. 7) we observe a third swap in the neutrinos between matter states 2 and 3, and the energies where we find the three splits are 2, 4 and 27–30 MeV. Finally, for just the 18.0 $M_\odot$ model, there is an additional soft split between neutrino matter states 1 and 2 at 26 MeV in the IH.

The anti-neutrinos display a sharp spectral split between states $\bar{1}$ and $\bar{3}$ for all three progenitors in the NH at energies of 24–26 MeV depending on the progenitor. In the IH all three models have an incomplete swap between anti-neutrino states $\bar{2}$ and $\bar{3}$ above ∼10–15 MeV.

What is remarkable about these figures is how similar they are even though the progenitors are very different. The results shown in Figures 6 and 7 are with luminosities and energies that appear to be far from the "standard" set of values [31, 33, 45, 50]. We find multiple splits in both hierarchies for both neutrinos and anti-neutrinos (depending on what time we are investigating). We give the luminosities, mean and rms energies for our models at 1 and 3 s in table III and we emphasize that the strong hierarchy in the luminosities seen in other simulations is not found here. Furthermore the energies are overall lower than in other simulations and the differences between the electron, anti-electron and non-electron flavor values are smaller. From the luminosities and mean energies given in table III we can also compute the number fluxes of neutrinos ($\Phi_f = L_{\nu_f}/E_{mean,\nu_f}$) which turns out to be very similar for all 3 progenitors. This explains why our results for the inner regions (Figures 6 and 7) are so relatively similar across our otherwise quite different progenitors. Likewise the density profiles of each model, shown in Fig. 1, are also very similar especially in the region $r \lesssim 200$ km. Since these 'inner region' calculations are collective dominated and the luminosities,

[1] We follow the terminology of A. Friedland (2010) [44] and define an incomplete swap to be when the survival probability is neither zero nor one, but instead decreases gradually with neutrino energy, i.e. the swap probability increases gradually with neutrino energy.

TABLE III. Luminosities and energies for our three progenitors at 1 and 3 s post bounce.

At 1 s:	8.8 $M_\odot$	10.8 $M_\odot$ (0.81 s)	18.0 $M_\odot$	At 3 s:	8.8 $M_\odot$	10.8 $M_\odot$ (2.82 s)	18.0 $M_\odot$
L_{ν_e} [10^{51} erg/s]	3.858	5.344	4.321		1.751	2.503	2.158
$L_{\bar{\nu}_e}$ [10^{51} erg/s]	3.826	5.410	4.537		1.617	2.276	2.056
L_{ν_x} [10^{51} erg/s]	4.382	6.271	5.292		1.969	2.863	2.539
$L_{\bar{\nu}_x}$ [10^{51} erg/s]	4.416	6.319	5.333		1.977	2.874	2.545
E_{mean,ν_e} [MeV]	9.189	10.19	9.322		8.804	9.890	9.007
$E_{mean,\bar{\nu}_e}$ [MeV]	11.72	12.90	11.73		10.55	11.82	10.77
E_{mean,ν_x} [MeV]	12.75	14.46	13.10		11.09	12.65	11.53
$E_{mean,\bar{\nu}_x}$ [MeV]	12.84	14.57	13.20		11.13	12.69	11.57
E_{rms,ν_e} [MeV]	10.26	11.37	10.42		9.848	11.12	10.10
$E_{rms,\bar{\nu}_e}$ [MeV]	13.20	14.48	13.20		12.15	13.64	12.38
E_{rms,ν_x} [MeV]	14.90	16.92	15.35		13.07	14.98	13.62
$E_{rms,\bar{\nu}_x}$ [MeV]	15.04	17.08	15.49		13.13	15.06	13.69

mean energies and profiles are so similar for each model, the results end up being very similar. If these collective features make their way through to the observed signal then from the viewpoint of decoding that signal the similarity is both good and bad: good in the sense that the features are robust and we can make definite statements about the neutrino hierarchy, but bad in the sense that there is no information about the star because the source seems to be standard.

2. *Outer region, 1000 km – profile end: MSW dominated*

Next we consider the evolution of the neutrinos through the outer layers of the star where the MSW effect takes over. Now the neutrino luminosities and mean energies are irrelevant and only the density profile matters. As shown in Fig. 1, the density profiles in the outer layers of the stars at 3 s pb are very different: The forward shock in the 8.8 $M_\odot$ model has raced off the simulation grid leaving a very steep density profile; The forward shock of the 10.8 $M_\odot$ model has propagated out to $r \sim 3\times10^4$ km and the presence of the forward shock, reverse shock and contact discontinuity are affecting the H resonances of the intermediate and higher energies and the L resonances of the lower, and in the 18.0 $M_\odot$ model the forward shock has propagated to a similar $r \sim 2 \times 10^4$ km but is only just beginning to affect the H resonances of the lower energies.

The question becomes whether these major differences in the profiles translate into equally different results for the neutrino transition probabilities through each progenitor. Our results for the outer region are shown Figures 8 (IH) and 9 (NH). Surprisingly we see the probabilities for the 8.8 $M_\odot$ and the 18.0 $M_\odot$ models at 3 s are virtually identical. The only difference are: In the 8.8 $M_\odot$ model a small amplitude undulation can be seen between 50 MeV and 100 MeV for anti-neutrinos in the IH and for the neutrinos in the NH; The 18.0 $M_\odot$ progenitor merely offers a small drop in the survival probabilities at ∼1–2 MeV for anti-neutrinos in the IH and for neutrinos in the NH. The drops in survival probabilities for the 18.0 $M_\odot$ model is caused by the lower portion of the forward shock just reaching into the resonant densities for low energy (anti-) neutrinos in the (inverted) normal hierarchy. Thus making their passage of the resonant densities diabatic leading to their enhanced flavor conversion. The reason the two sets of results are so similar is because the neutrino evolution through both profiles is very close to adiabatic despite the very different gradients of the density at the H and L resonances of each progenitor. The adiabaticity of the L resonance for supernova neutrinos has been long known but the adiabaticity of the H resonance is dependent upon the mixing angle θ_{13} and until recently this angle was unknown. The measurement of a relatively large value for θ_{13} means that neutrinos experiencing a single, non-shock related, H resonance will do so adiabatically giving no flavor conversion.

In contrast the 10.8 $M_\odot$ model is a lot more interesting. Starting with the anti-neutrinos in the IH, we see an incomplete shock-induced split between states $\bar{1}$ and $\bar{3}$ at 3.5 MeV. Above 40 MeV is an additional incomplete swap between states $\bar{1}$ and $\bar{3}$. Furthermore we see sharp changes in the average survival probability of states $\bar{1}$ and $\bar{3}$ at 10 MeV and ∼12 MeV. The anti-neutrino state $\bar{2}$ has a small dip in the survival probability at ∼3 MeV. A slightly larger dip is visible for neutrinos in the IH in the survival probabilities of matter states 1 and 2 at ∼3 MeV. When we turn to the NH, we see that a similar small dip is present in the survival probabilities of anti-neutrino states $\bar{1}$ and $\bar{2}$ at ∼3 MeV. In the NH the neutrinos now have the interesting features. We see an incomplete shock-induced split between neutrino states 2 and 3 at 3.5 MeV, and above 40 MeV we see another incomplete swap. A careful study also reveals that the average survival probability of neutrino states 2 and 3 increase abruptly at roughly 24 MeV.

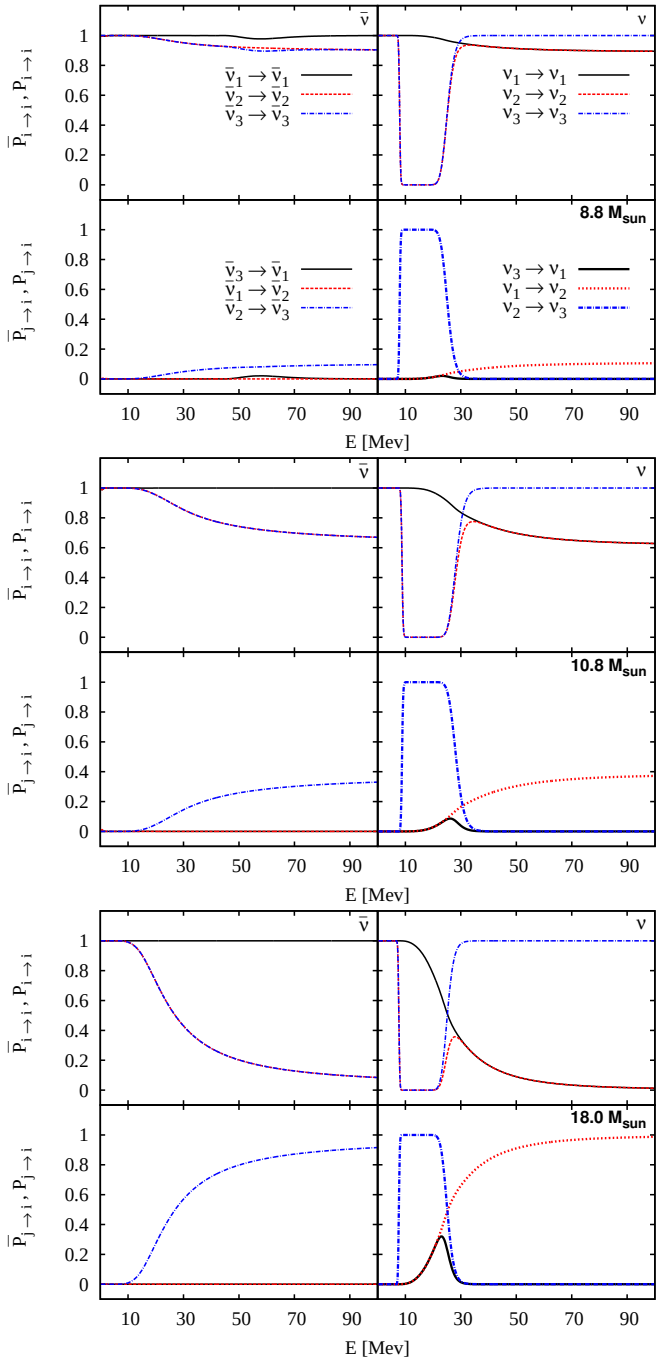

FIG. 6. (color online). Matter state survival and transition probabilities at 3 s pb for $\bar{\nu}$ (*left panels*, $\bar{P}$) and ν (*right panels*, P) in the Inverted Hierarchy for the inner region. The top four panels belong to the 8.8 $M_\odot$ model, the middle four to the 10.8 $M_\odot$ progenitor and the bottom four to the 18.0 $M_\odot$ progenitor. Matter survival probabilities $P_{\nu_i\to\nu_i}$ are shown in the upper panels of each quartet, and transition probabilities $P_{\nu_i\to\nu_j}$ are shown in the bottom ones. The solid black lines indicate the probabilities for ending in matter state 1 (or anti-matter state $\bar{1}$ in the case of anti-neutrinos), the red dashed lines give the probabilities of ending in matter state 2 ($\bar{2}$) and finally the blue dot-dashed lines give the probabilities for ending in matter state 3 ($\bar{3}$) at the end of the calculation domain. See the text for more explanation.

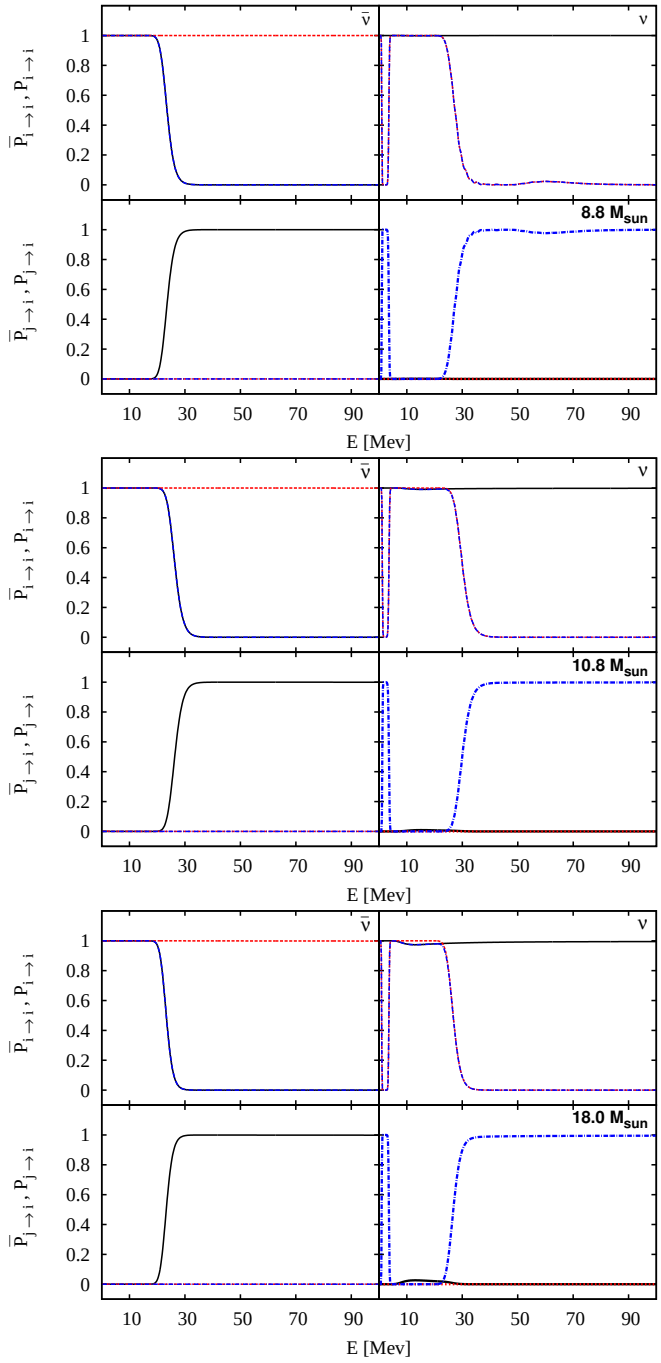

FIG. 7. (color online). Matter state survival and transition probabilities at 3 s pb for $\bar{\nu}$ (*left panels*, $\bar{P}$) and ν (*right panels*, P) in the Normal Hierarchy for the inner region. The top four panels belong to the 8.8 $M_\odot$ model, the middle four to the 10.8 $M_\odot$ progenitor and the bottom four to the 18.0 $M_\odot$ progenitor. Matter survival probabilities $P_{\nu_i\to\nu_i}$ are shown in the upper panels of each quartet, and transition probabilities $P_{\nu_i\to\nu_j}$ are shown in the bottom ones. The solid black lines indicate the probabilities for ending in matter state 1 (or anti-matter state $\bar{1}$ in the case of anti-neutrinos), the red dashed lines give the probabilities of ending in matter state 2 ($\bar{2}$) and finally the blue dot-dashed lines give the probabilities for ending in matter state 3 ($\bar{3}$) at the end of the calculation domain.

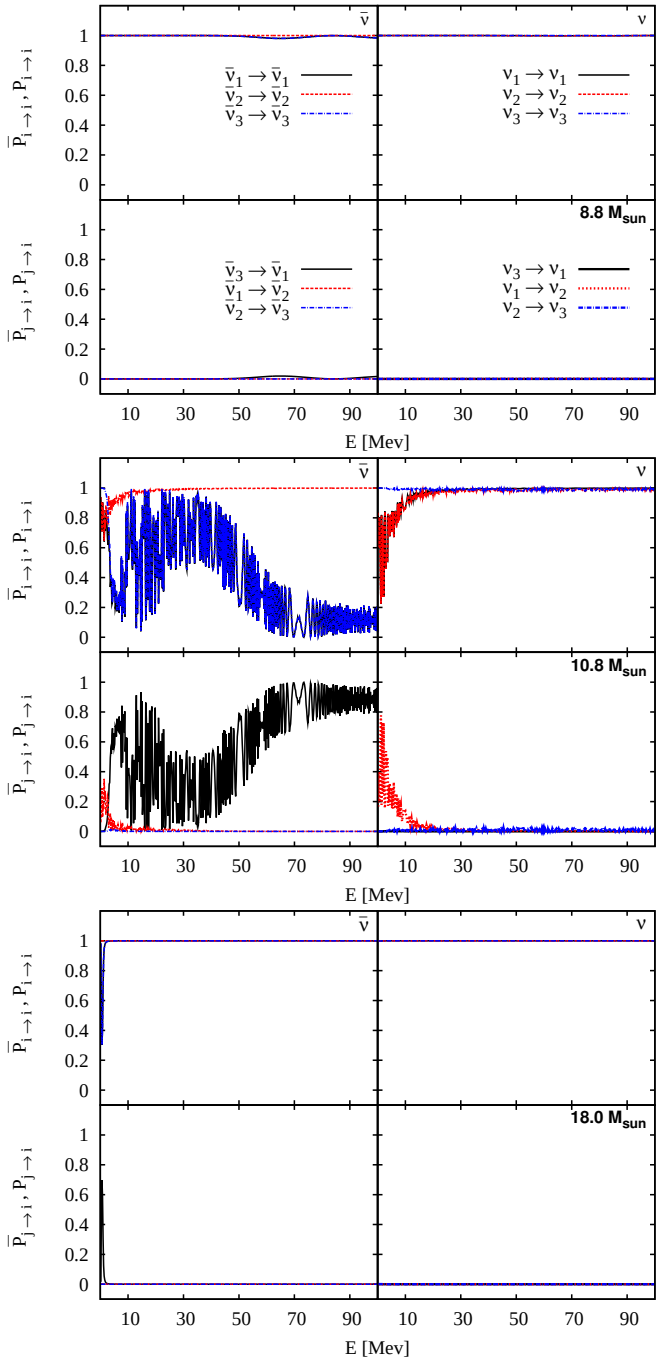

FIG. 8. (color online). As Fig. 6 but for the outer region. Inverted Hierarchy.

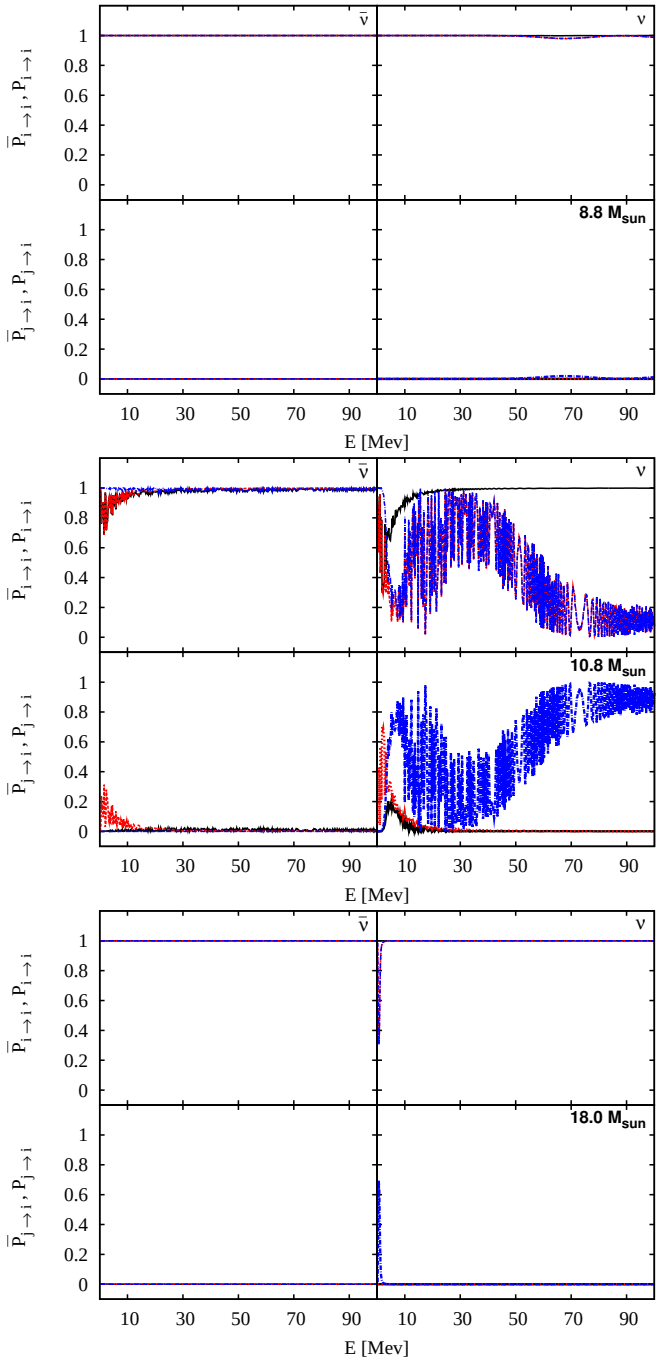

FIG. 9. (color online). As Fig. 7 but for the outer region. Normal Hierarchy.

In both hierarchies we see phase effects [90, 91] on top of the aforementioned swaps. In the IH there are large phase effects in the anti-neutrino states $\bar{1}$ and $\bar{3}$, but also for the neutrino states 1 and 2 do we see phase effects at low energies. In the NH the large phase effects are visible in the neutrino states 2 and 3, and only smaller effects are visible in the anti-neutrino states $\bar{1}$ and $\bar{2}$ for lower energies. Contrary to Dasgupta & Dighe [91], who only see phase effects for neutrinos in the NH and for anti-neutrinos in the IH, we thus find phase effects for neutrinos and anti-neutrinos in both hierarchies. We note that the feature around ∼71 MeV in the IH anti-neutrinos and around ∼73 MeV in the NH neutrinos is an effect of the phase effect being close to resonance at these energies (A similar feature is seen in Fig. 2 of [61]). The drops in survival probabilities seen for neutrino states 1 and 2 at roughly 3.5 MeV in both hierarchies, are actually the first little effects of the shock hitting the MSW L

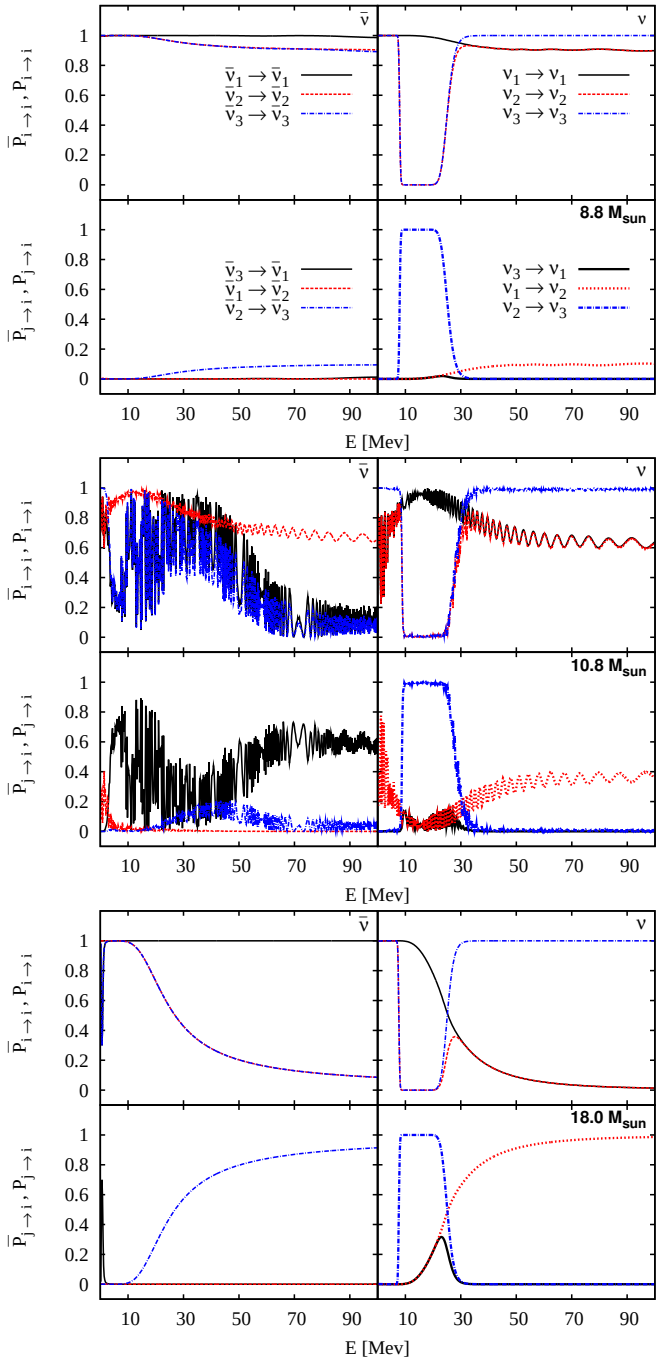

FIG. 10. (color online). As Fig. 6 but for the full profile traversal. Inverted Hierarchy.

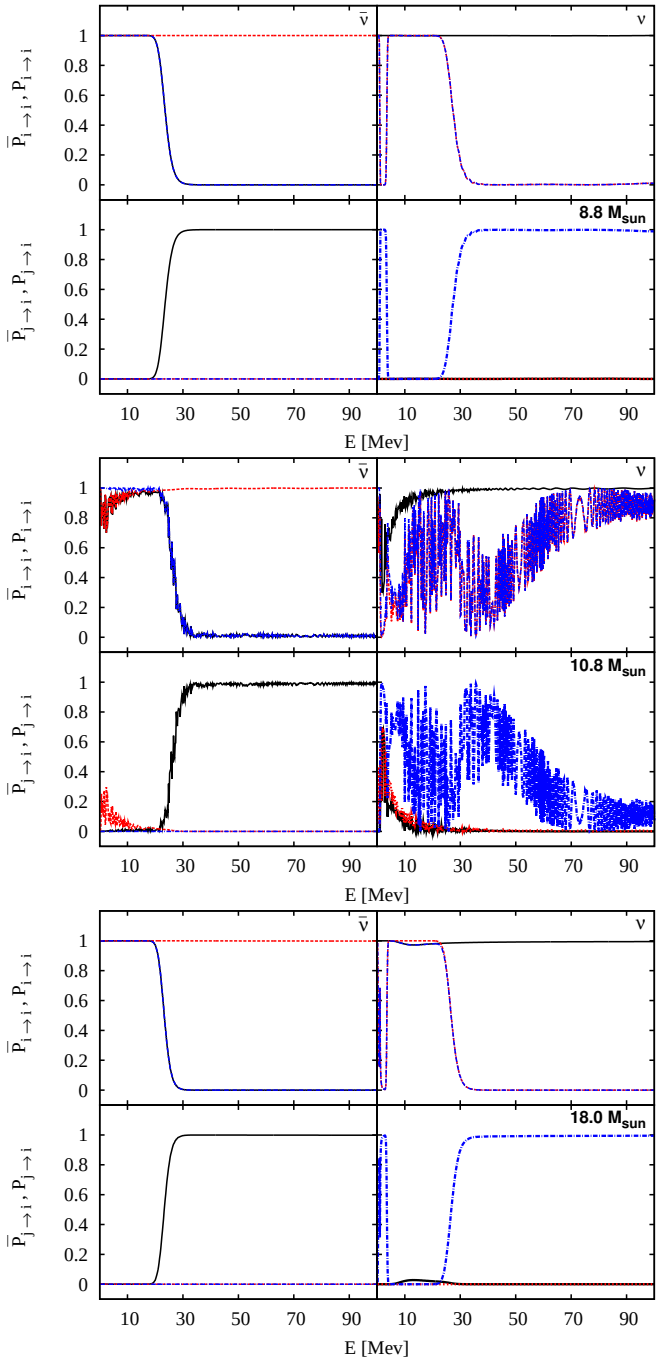

FIG. 11. (color online). As Fig. 7 but for the full profile traversal. Normal Hierarchy.

resonance. The magnitude of the drops are similar in the two hierarchies, as we would expect, although the effect is enhanced and somewhat obscured in the NH, where state 2 also mix with state 3 through the H resonance. We are the first ones to follow the shock wave out to densities relevant for the MSW L resonance, and calculate the flavor probabilities in this region. We will go into further detail with these findings in Sec. IV.

3. *Full profile traversal*

The two previous calculations showed separately how the collective and MSW effects generate features in the spectrum. Now we put the two together and show in Figures 10 and 11 the results of calculations covering the entire density profile from PNS surface to the end.

In a broad sense the results display phenomena which are consistent in most of the profiles we have investigated.

In a full calculation the splits and swaps induced in the inner and outer regions respectively are now combined in a superposition. All the features present in the inner region can be recovered, as well as the features from the outer region. The clean superposition is evident in the cases of the 8.8 $M_\odot$ and 18.0 $M_\odot$ models where very little happens in the outer region, which can be seen by comparing Figures 10 and 11 with Figures 6, 7, 8 and 9.

A slightly different story is visible in the middle panels for the 10.8 $M_\odot$ model in Figures 10 and 11. We see the superposition but new features have also emerged. In broad terms we can divide the probabilities into 3 categories: i) those that remain the same as they were either in the inner region or in the outer region; ii) those that are a simple superposition - below a certain energy they follow the trend seen in the outer region calculation while above that energy they follow the trends of the inner region; iii) the complex cases that are neither i) nor ii).

By comparing the middle quartet of Fig. 10 (IH) to the ones of Fig. 6 and Fig. 8 we see that $\bar{P}_{11}$ is an example of case i) because it follows its path from the outer region and nothing happened to $\bar{\nu}_1$ in the inner region. Similarly P_{33} is another case i) example because it follows its trend from the inner region, albeit with minimal fluctuations on top, since very little happens to ν_3 in the outer region. The three probabilities $\bar{P}_{22}$, P_{11} and P_{22} are all case ii) because we see that each of these probabilities follow the same pattern as in the outer region (Fig. 8) below an energy of 12, 15 and 8 MeV respectively while above these energies they follow the trend they developed in the inner region (Fig. 6). Additionally, for all three probabilities new small amplitude oscillations have arisen. At higher energies the oscillations have a larger frequency, than at lower energies. Finally $\bar{P}_{33}$ falls into the more complex, case iii) category: Below 25 MeV it follows the pattern from the outer region, above this energy it has the same oscillations it displayed in the outer region it just falls off slightly quicker, so that at higher energies the average survival probability is slightly lower.

Turning to the NH and comparing quartets of Fig. 11 to Figures 7 and 9 we find that P_{11} is a case i) example as it follows its trend from the outer region, although with oscillations of tiny amplitude above 30 MeV. $\bar{P}_{33}$ too is a case i) as it follows its trend from the inner region, but with additional minor random fluctuations superimposed which arise in the outer region. Both $\bar{P}_{11}$ and $\bar{P}_{22}$ belong to case ii) as they follow their pattern from the outer region below 20 MeV, and change to follow the pattern from the inner region above this energy, albeit with slight fluctuations. This leaves us with P_{22} and P_{33} belonging to case iii) who are slightly more complex, and share a common story. They both display the splits at 2 and 4 MeV that arose in the inner region, although the latter split is no longer complete, because an additional incomplete swap is caused in the outer region. Between 4 MeV and 30 MeV the probabilities follow the pattern they had in the outer region. Above 30 MeV the spectral split from the self-interaction in the inner region has swapped the spectra of ν_2 and ν_3 completely. When they then propagate through the outer region the MSW effect swaps them again, but this time incompletely. Therefore we see an abrupt drop in the probabilities at 30 MeV, and above this energy the probabilities appear as a reflected version of the pattern present for the outer region alone.

So, in summary, we see that the combination of collective and MSW effects often produces results which are consistent with a trivial superposition and in other cases the combined effect results in a new feature. The exact reason needs to be explored more carefully but at the same time it is not entirely unexpected or unprecedented. The S matrix describing the calculation for the entire profile is the product of the S matrices computed for the inner region S_I and the outer region S_O: $S = S_O\, S_I$. Both S_O and S_I are of the form

$$S = \begin{pmatrix} \alpha_1 & \alpha_2 & \alpha_3 \\ \frac{-D\alpha_2^*\alpha_5^* - \alpha_1\alpha_4\alpha_3^*}{1-|\alpha_3|^2} & \frac{D\alpha_1^*\alpha_5^* - \alpha_2\alpha_4\alpha_3^*}{1-|\alpha_3|^2} & \alpha_4 \\ \frac{-D\alpha_2^*\alpha_4^* - \alpha_1\alpha_5\alpha_3^*}{1-|\alpha_3|^2} & \frac{D\alpha_1^*\alpha_4^* - \alpha_2\alpha_5\alpha_3^*}{1-|\alpha_3|^2} & \alpha_5 \end{pmatrix} \qquad (4)$$

where the α_i's are complex numbers with the requirement that $|\alpha_1|^2+|\alpha_2|^2+|\alpha_3|^2 = |\alpha_3|^2+|\alpha_4|^2+|\alpha_5|^2 = 1$ and D is the determinant of unit magnitude. Multiplying two matrices of this form together leads to a very messy expression in general which only gets worse when one computes the square amplitudes of the matrix elements so as to produce the transition probabilities. The only simple case is the element S_{13} whose product is $S_{13} = \alpha_1^{(O)}\,\alpha_3^{(I)} + \alpha_2^{(O)}\,\alpha_4^{(I)} + \alpha_3^{(O)}\,\alpha_5^{(I)}$. The transition probability $P_{13} = |S_{13}|^2$ is of the form $P_{13} = P_{11}^{(O)}\,P_{13}^{(I)} + P_{12}^{(O)}\,P_{23}^{(I)} + P_{13}^{(O)}\,P_{33}^{(I)} + \ldots$ where the $P_{ij}^{(R)}$ are the transition probabilities between states j and i in region R. The term $P_{11}^{(O)}\,P_{13}^{(I)} + P_{12}^{(O)}\,P_{23}^{(I)} + P_{13}^{(O)}\,P_{33}^{(I)}$ is exactly what we expect from a straight superposition of probabilities but in addition there are many extra terms, which we have not explicitly written out, which depend upon both the phases and magnitudes of the α's. These phase terms are due to 'interference' between the collective and MSW calculations and a sign of this interference is that the new features found when we combine the calculations are oscillatory as a function of energy as the interference varies from constructive to destructive and back again.

4. *Including turbulence*

Finally we consider the results from our fourth set of calculations where the neutrinos again traverse the full profile but now with added turbulence. These are shown in Figures 12 and 13. From the way we have included turbulence (see Sec. II C) the results of the 8.8 $M_\odot$ and 18.0 $M_\odot$ are more directly comparable but quite generally adding 10% ($C_* = 0.1$) turbulence to our density

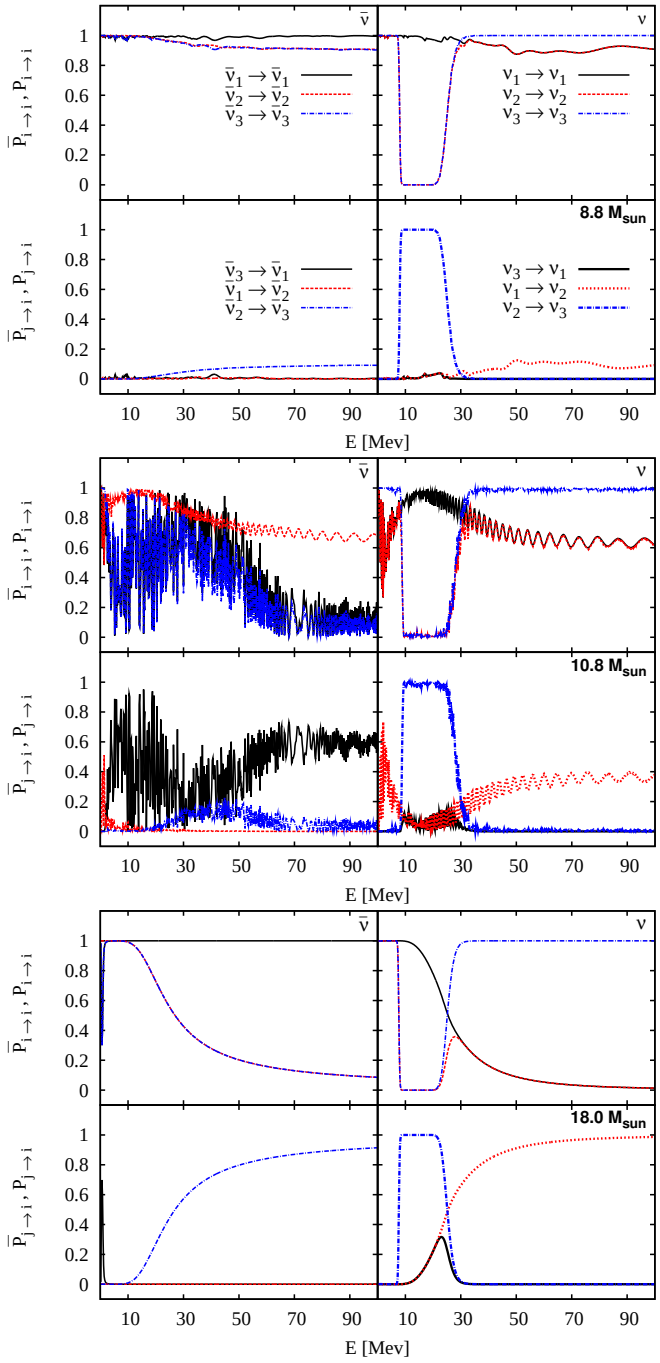

FIG. 12. (color online). As Fig. 6 but for the full profile traversal with 10% turbulence added. Inverted Hierarchy.

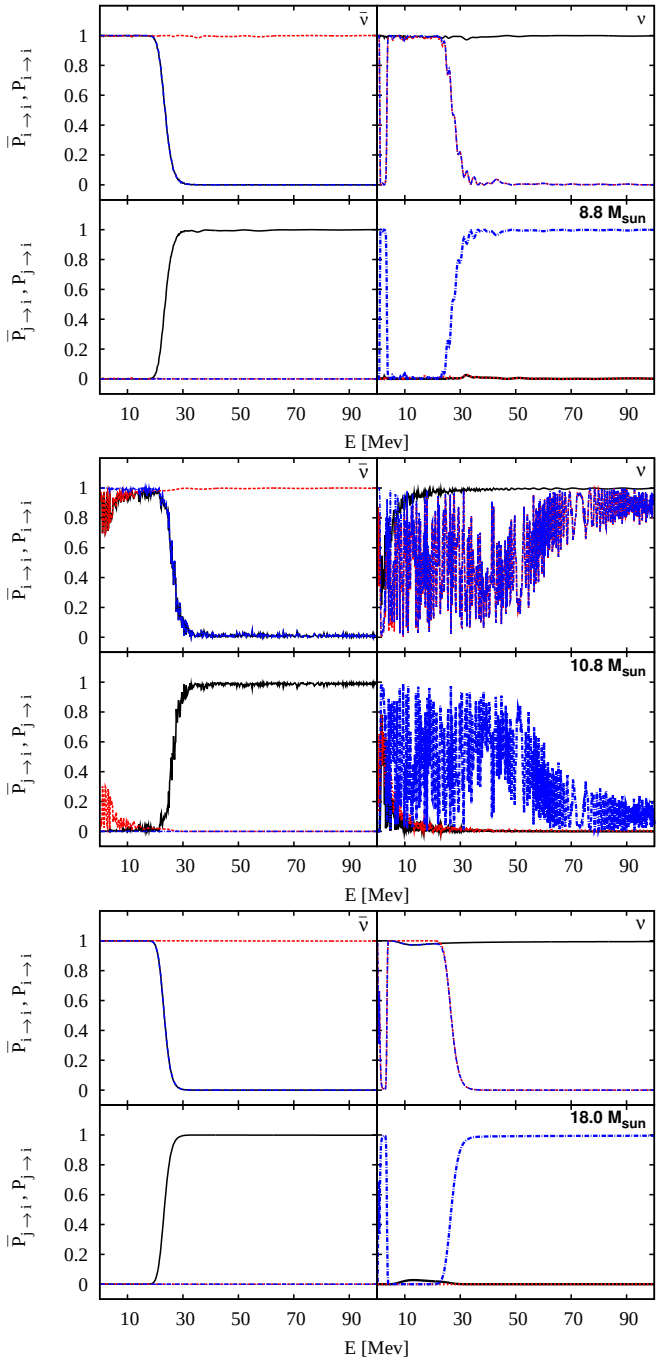

FIG. 13. (color online). As Fig. 7 but for the full profile traversal with 10% turbulence added. Normal Hierarchy.

profiles at 3 s does not lead to dramatic changes. When we look closely, though, we see that minor alterations have occurred. Focusing our attention on $\bar{P}_{22}$ for the 10.8 $M_\odot$ model in Fig. 12, we see that at 100 MeV the endpoint of the red dashed line bends the opposite way of what it does in Fig. 10. This indicates that turbulence in this case acts as to introduce an additional phase effect. The clear transition points at 30 MeV that were visible in P_{22}, P_{33} and P_{32} in Fig. 11 for the 10.8 $M_\odot$ model have been obscured by the bigger amplitudes of the phase effects introduced by the addition of turbulence. Generally the effect of adding a moderate amount of turbulence to this profile can be summarized as an increase in the amplitudes of the phase effect oscillations, and a slight shift in the position of these.

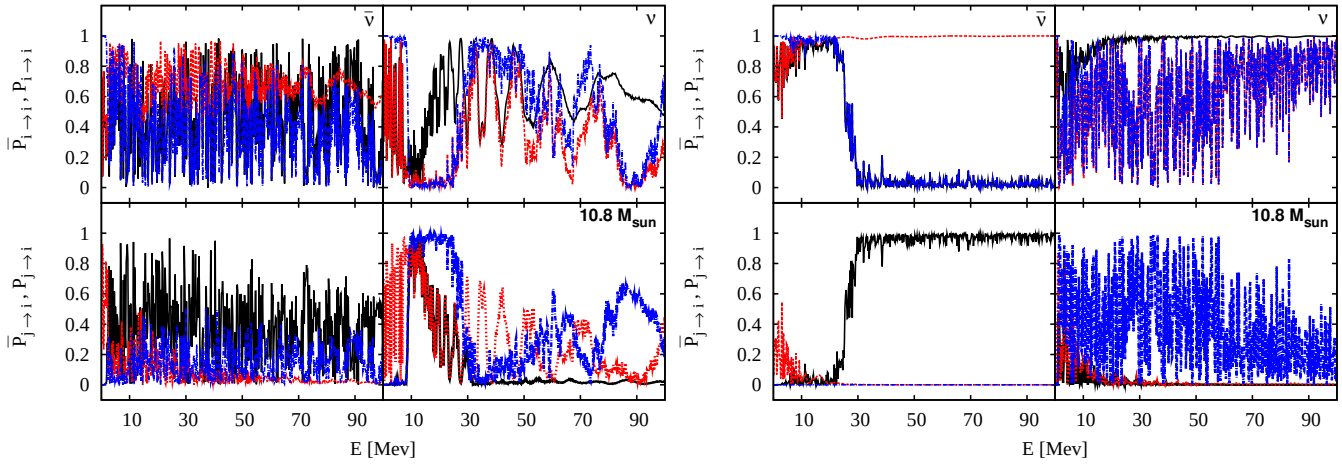

FIG. 14. (color online). Matter survival and transition probabilities at 2.8 s with 30% turbulence for the 10.8 $M_\odot$ model. In the four panels on the left we show the IH and in the four panels on the right we show the NH. Lines and layout as before.

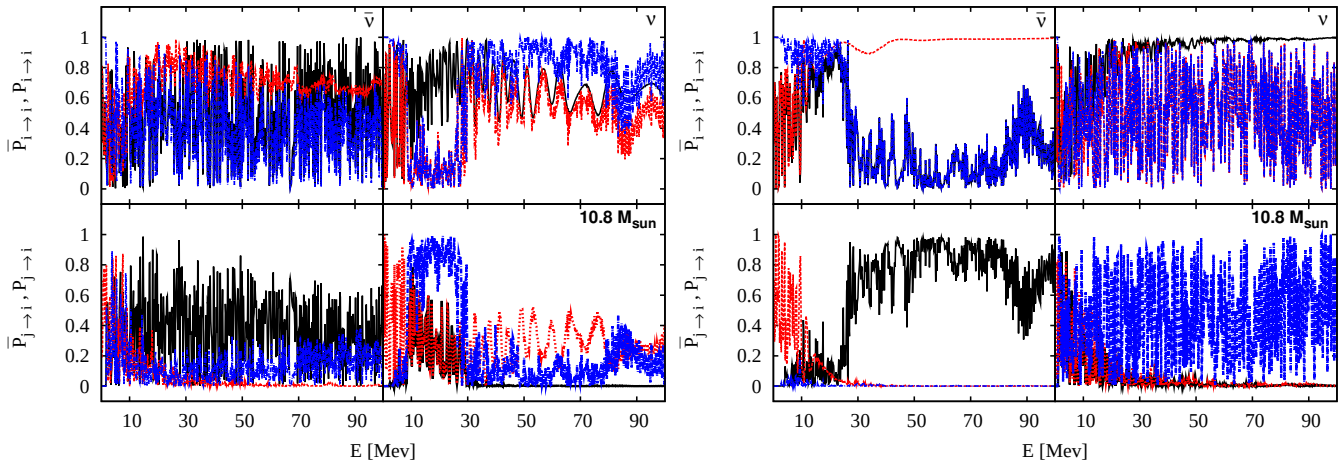

FIG. 15. (color online). As Fig. 14 but with 50% turbulence instead of 30%.

5. *Larger Turbulence*

So far we have investigated a turbulence amplitude of 10% and seen in the previous section that it has rather limited effect. The reason is that we are using a value of θ_{13} in line with the present measurements which tends to make H resonances more adiabatic [73]. Turbulence amplitudes of 10% are the most one might expect to occur in ONeMg supernovae such as the 8.8 $M_\odot$ model because even spherical simulations of these supernovae successfully explode. But in contrast, for more massive progenitors spherical models do not explode and multi-dimensional physics of some kind is necessary. Such circumstances would naturally lead to aspherical explosions and the generation of large amplitude turbulence. Therefore we extended the investigation for the 3 sec profile to 30% and 50% turbulence ($C_* = 0.3$ and 0.5). For these investigations we primarily focused on the 10.8 $M_\odot$ model, but we have also done calculations for the 18.0 $M_\odot$ model with 30 and 50% turbulence.

It is evident from Figures 14 and 15 that a number of the main superposed collective and MSW features remain but the amplitude of the phase effect oscillations increase, and we also see a shift in some of the high frequency oscillations. The most interesting part of Figures 14 and 15 is that for both levels of turbulence it is always possible to identify the two spectral splits in neutrino states 2 and 3 in the IH, and the single split in anti-neutrino states $\bar{1}$ and $\bar{3}$ in the NH, although as a general rule the amplitude of all fluctuations increases with turbulence increasing from 10% to 30% and 50%. This increase in fluctuation amplitude makes it impossible to identify the trends visible in the full profile results for anti-neutrinos in the IH, and it gradually obscures the split in the NH between neutrino states 2 and 3, until not even the high energy trend is visible at 50% turbulence. In the IH additional large amplitude, low frequency oscillations arises at high energies in the neutrino probabilities as the turbulence is increased.

By comparing the upper left panel of the right quartet

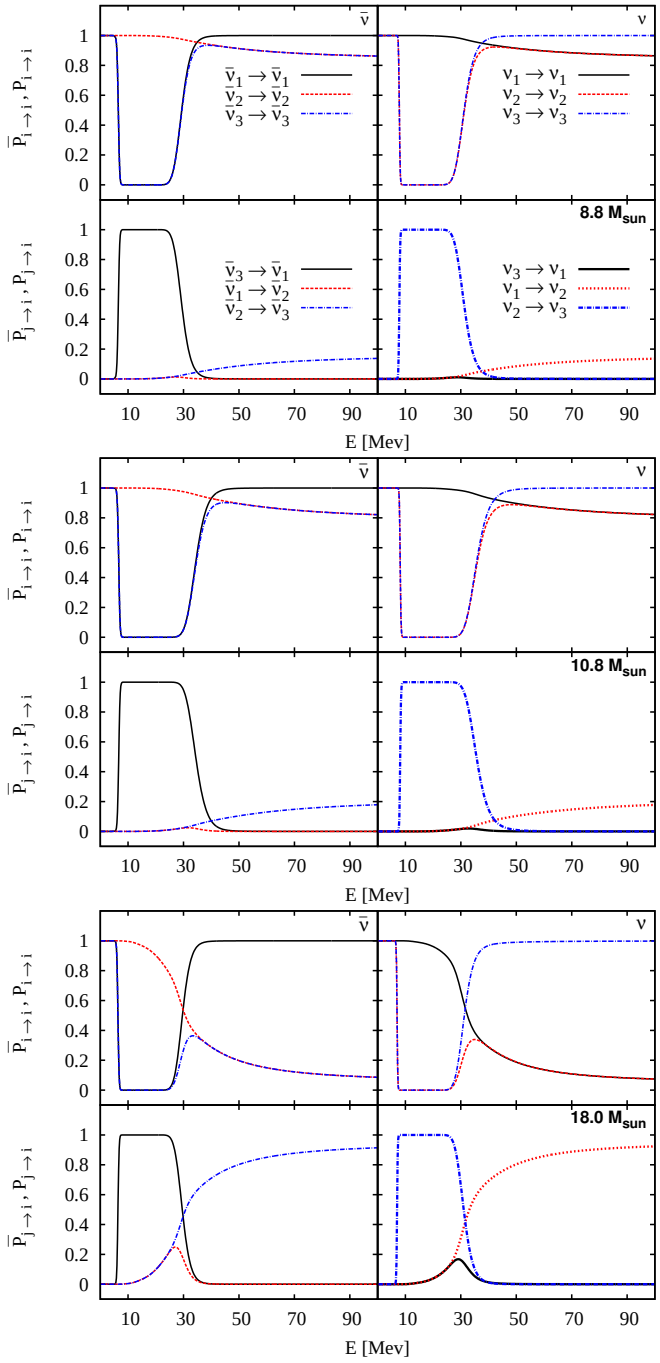

FIG. 16. (color online). As Fig. 6 but for 1 s pb. Results from the inner region in the IH. Lines and layout as before.

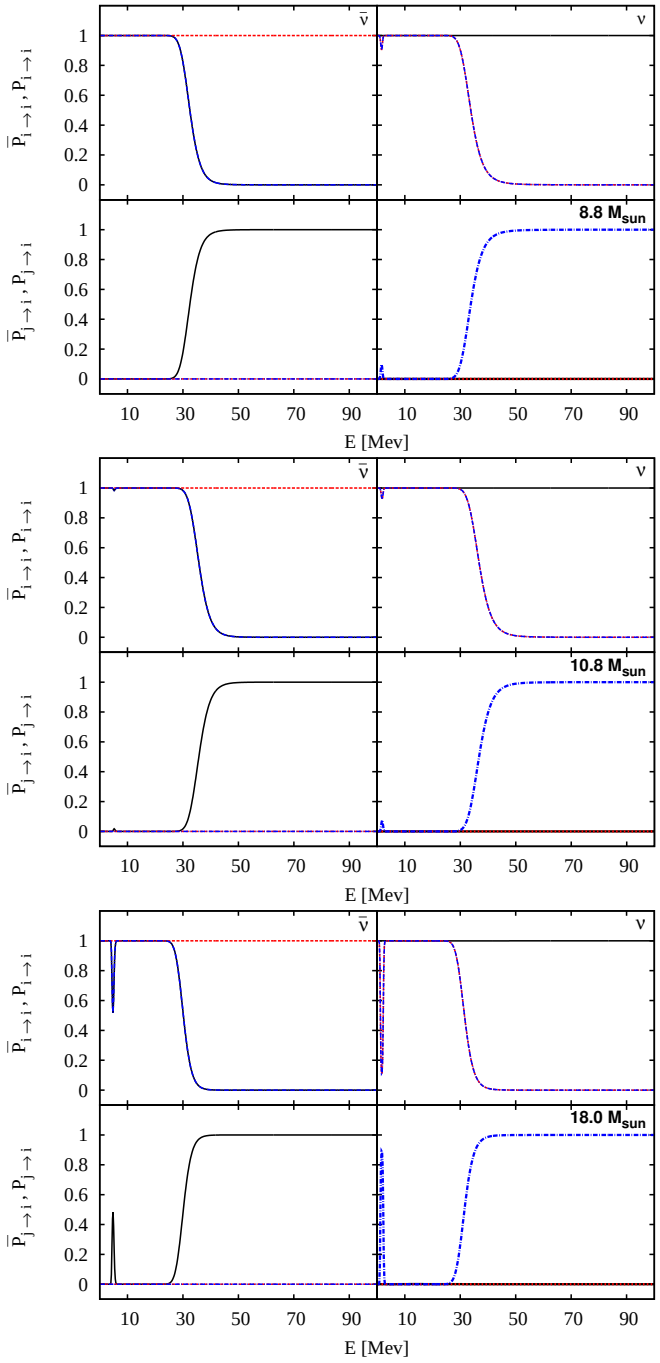

FIG. 17. (color online). As Fig. 7 but for 1 s pb. Results from the inner region in the NH. Lines and layout as before.

in Fig. 14 (anti-neutrino survival probabilities) with the one in Fig. 15 we see that although the survival probability of both anti-neutrino states $\bar{1}$ and $\bar{3}$ drops above 30 MeV, then in Fig. 14 they drop to zero but in Fig. 15 the average probabilities only drops to about 0.2. From the transition probabilities (lower left panels) we see that the probability for anti-neutrino state $\bar{3}$ to go into state $\bar{1}$ has fallen from 100% to an average of 80% when the turbulence was increased. Thus instead of completely converting states $\bar{1}$ and $\bar{3}$ into one another, we now have a small admixture of the original state. At the PNS an $\bar{\nu}_e$ is created in matter state $\bar{\nu}_3$ in the NH but it will travel predominantly as mass state $\bar{\nu}_1$ in vacuum. From the transition probabilities we see that this means 80% of the $\bar{\nu}_3$ state gets converted into $\bar{\nu}_1$, which means it stays as an $\bar{\nu}_e$. Naturally this entails that about 20% of the energy spectrum from neutrinos initially created as $\bar{\nu}_x$ will be mixed in with about 80% of the energy spectrum

of neutrinos initially created as $\bar{\nu}_e$ (aka $\bar{\nu}_3$) to form the final energy spectrum of the state we would observe as $\bar{\nu}_e$ (aka $\bar{\nu}_1$).

As this conversion is happening at the higher energies, above 30 MeV, we get the higher energy non-electron flavor contribution added to the spectrum, increasing the number of higher energy neutrinos, which with current detector technology is the easiest to observe.

B. Profiles at 1 second

1. *Inner region, 70 – 1000 km: Collective dominated*

Now that we understand how the various neutrino flavor transformation effects combine we can turn our attention to the density profiles at other times. We begin with density profiles at 1 s pb, and the calculation results for the inner, collective dominated, region are shown in Figures 16 and 17. The line colors and styles are the same as in Figures 6 and 7.

Let us focus on the anti-neutrinos first. For the IH (Fig. 16) a common trait in all three models is a spectral split at a very low energy ($\sim$ 5–7 MeV) and a second split at an intermediate energy ($\sim$ 30–35 MeV) in the anti-neutrino states $\bar{1}$ and $\bar{3}$. From the top left panels of each quartet we see that between these two energies the survival probabilities of the two states drop to zero. For anti-neutrino states $\bar{3}$ and $\bar{2}$ we also see a decrease in survival probability at energies above $\sim$ 35–40 MeV. From the transition probability plots we infer that at these energies the anti-neutrino states $\bar{2}$ and $\bar{3}$ have made an incomplete swap. In the case of the two lighter models this incomplete swap is very small, but for the 18.0 $M_\odot$ model the incomplete swap is significant and approaches a full swap, and starts at a slightly lower energy.

In the NH (Fig. 17) we again see a common feature across the progenitors: a complete swap of anti-neutrino states $\bar{1}$ and $\bar{3}$ at an energy of $\sim$ 30–35 MeV. For neutrinos we see the same feature in the same energy range, but now between matter states 2 and 3. They also show additional dips in the survival probabilities at energies of 2–5 MeV for matter states 2 and 3 for all three models. The 18.0 $M_\odot$ model show a similar feature in the anti-neutrino states $\bar{2}$ and $\bar{3}$ at the same energy.

In the IH neutrinos show multiple interesting features as evident from the right panels of Fig. 16. The most prominent features are two spectral splits at $\sim$ 7–8 MeV and $\sim$ 31–36 MeV between matter states 2 and 3, leading to a full swap of the two states in the energy region in-between. This is not unlike the splits seen between states $\bar{1}$ and $\bar{3}$ in the anti-neutrinos. As in the anti-neutrino case the 18.0 $M_\odot$ progenitor has an additional swap in the neutrinos. This time the swap occurs at an energy of $\sim$ 30 MeV and between matter states 1 and 2.

Although the quartets for the 8.8 and 10.8 $M_\odot$ models appear quite similar they are in fact different. This is most easily seen at the crossing point between P_{11} and P_{33} near 35 MeV in the upper right panel for the 8.8 $M_\odot$ model, which are found at 40 MeV for the 10.8 $M_\odot$ model.

The similarity of the probabilities across the three progenitors is again striking. The explanation follows the same lines as for the 3 s results. The ratios between the fluxes of ν_e and ν_x, as well as between $\bar{\nu}_e$ and $\bar{\nu}_x$, are as similar for the three progenitors at 1 s as they were at 3 s, which can be easily computed from the luminosities and mean energies given i table III. The overall flux ratios are about 10% higher at 1 s than at 3 s so we would expect the collective interaction to be stronger which is what we see. The larger interaction strength explains why we see full swaps between anti-neutrino states $\bar{1}$ and $\bar{3}$ in the IH at 1 s and why those swaps have disappeared at 3 s. Furthermore, at 1 s the density profiles of the 10.8 $M_\odot$ and the 18.0 $M_\odot$ models are almost identical out to $\sim$700 km (upper panel of Fig. 1). The 8.8 $M_\odot$ density profile follows the other two closely out to 100 km where after it falls off much quicker. The similarity of the density profiles thus corroborate the similarity of the results for the three progenitors.

Comparing in more detail the results from the calculations of the inner region at 1 s to the ones at 3 s, we find that the spectral split between $\bar{1}$ and $\bar{3}$ in the NH is present at both 1 and 3 s but has moved from an energy of 30–36 MeV at 1 s to 24–26 MeV at 3 seconds (Compare Figures 16 and 17 with Figures 6 and 7). The split between neutrino states 2 and 3 in the NH has likewise moved down in energy from 32–37 MeV at 1 s to 27–30 MeV at 3 s, and of the two splits present in neutrino states 2 and 3 the lower one at 7–8 MeV remains in place, but the one at higher energies has moved down from 31–36 MeV to 24–28 MeV from 1 s to 3 s. The explanation of the movement in energy of the spectral splits is unclear, but the movement continues over time as is shown in Sect. IV. Counter intuitively the small dip in the survival probabilities P_{22} and P_{33} at $\sim$ 2 MeV grow into a full double split from 1 to 3 s although the fluxes fall off by 10% and the interaction strength would be expected to diminish too. In the IH the incomplete swaps in the anti-neutrino states $\bar{2}$ and $\bar{3}$ above 30 MeV persist from 1 to 3 s.

From the top panel of Fig. 1 we clearly see that within 1000 km the 1 s density profiles of models 10.8 $M_\odot$ and 18.0 $M_\odot$ have values at least a magnitude larger than the resonant densities for the MSW effect. We therefore conclude that all the effects we observe in these two cases must be caused by collective effects. Furthermore, since the traversal of the high density MSW resonance that do take place is adiabatic for the 8.8 $M_\odot$ model, and the probability plots show such similarities to the ones for the 10.8 $M_\odot$ model, we conclude that the changes in probabilities are also in this case caused by collective effects.

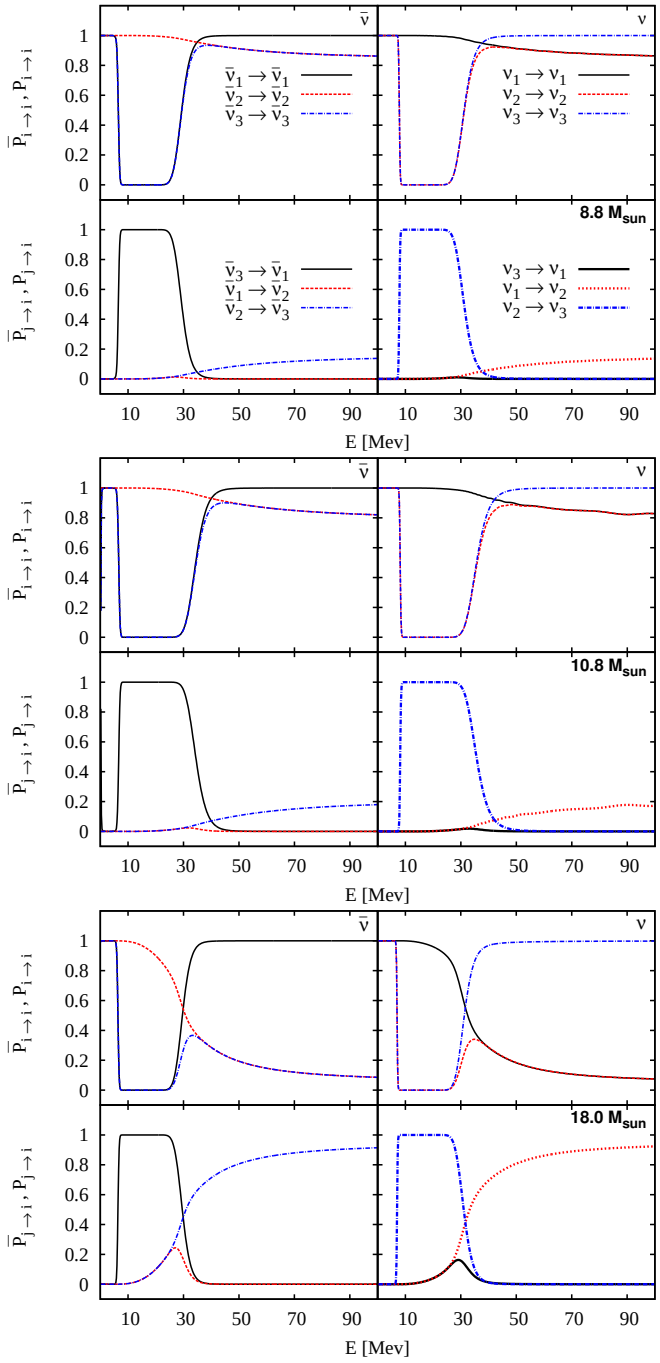

FIG. 18. (color online). As Fig. 16 but for the full profile traversal. Inverted Hierarchy.

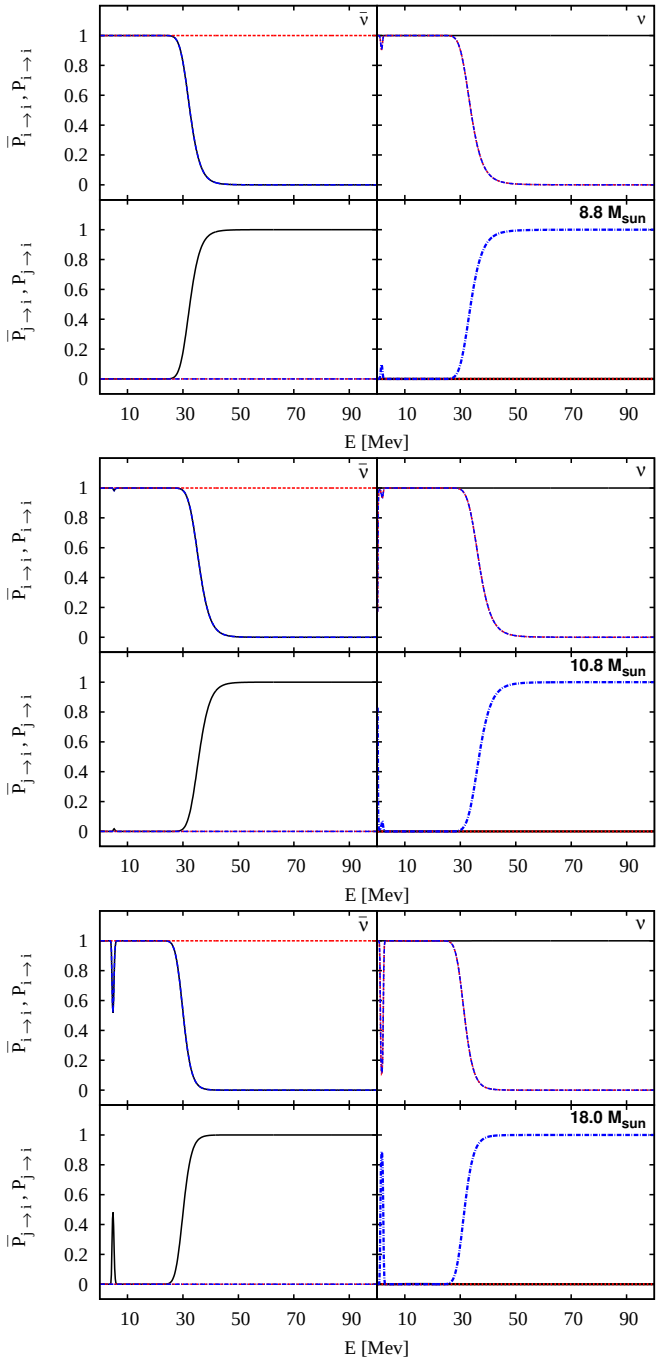

FIG. 19. (color online). As Fig. 17 but for the full profile traversal. Normal Hierarchy.

2. Outer region, 1000 km – profile end: MSW dominated

At this relatively early time we see no significant evolution of the matter states as they travel through the outer region. The survival probabilities stays mainly at unity. Therefore we do not include figures of the results of our calculations for this region. Only for the 10.8 $M_\odot$ model do we see a dip in the survival probabilities for the anti-neutrino states $\bar{1}$ and $\bar{3}$ at an energy of ~ 1 MeV in the IH, and at the same energy for the neutrinos in the NH where matter states 2 and 3 transition into one another.

The lack of interesting effects in this region is easily understood by consulting the top panel of Fig. 1: The shocks and the contact discontinuity are at densities well above the resonant densities for the MSW effect. The H and L resonant densities are therefore traversed adiabatically by the neutrinos, if the density profile reaches the relevant density levels. This is unlike the profile at

3 seconds (lower panel of Fig. 1) where the shocks are in the resonant density area, and MSW effects can be seen in the probabilities. Comparing the results at 1 s with the results from 3 s (Sec. III A Figures 8 and 9) for the outer MSW dominated region, clearly shows how the MSW impact rises over time as the shocks move into the relevant density regions. Hardly any effect of the MSW is present at 1 s, but at 3 s we see changes in the probabilities from both the H and L MSW resonances. This will be discussed further in Sec. IV.

3. *Full profile traversal*

For the full profile traversal we observe that the probabilities are a superposition of the ones from the inner and outer region, the same result as we found for the 3 sec profiles. The probabilities for the full calculations are shown in Figures 18 (IH) and 19 (NH). Since nothing significant happens in the outer region they reflect the flavor conversions occurring in the inner region.

The differences between results from 1 and 3 s in each of the inner and outer regions separately are naturally also reflected in the full calculations.

4. *Including turbulence*

Finally in Figures 20 and 21 we show the results of calculations where turbulence has been included as the neutrino traverses the full profile. For the 10.8 $M_\odot$ and the 18.0 $M_\odot$ progenitor the addition of 10% turbulence to this profile has no impact on the survival and transition probabilities as can be seen by comparing Fig. 18 with Fig. 20, and Fig. 19 with Fig. 21. For the 8.8 $M_\odot$ progenitor the story is quite different. We see distinct imprints in 9 out of 12 survival probabilities. The unchanged probabilities are $\bar{P}_{22,\mathrm{IH}}$, $\bar{P}_{22,\mathrm{NH}}$ and $P_{33,\mathrm{NH}}$, while $P_{11,\mathrm{IH}}$, $P_{22,\mathrm{IH}}$, $P_{33,\mathrm{IH}}$, $\bar{P}_{11,\mathrm{NH}}$ and $\bar{P}_{33,\mathrm{IH}}$ show only small amplitude oscillations as changes. Finally $\bar{P}_{11,\mathrm{IH}}$, $\bar{P}_{33,\mathrm{NH}}$, $P_{22,\mathrm{NH}}$ and $P_{33,\mathrm{NH}}$ all show large amplitude oscillatory behavior on top of their still clearly visible spectral splits.

The addition of turbulence has such a profound effect on the 8.8 $M_\odot$ model because the density profile at 1 s is relatively flat (see the upper panel of Fig. 1). The addition of even low amplitude turbulence effectively creates a multitude of H resonances compared to the case without turbulence. By comparing the panels for the 8.8 $M_\odot$ model in Figures 18 and 20, and Figures 19 and 21, we see that, as expected, the new resonances impact primarily the anti-neutrino states $\bar{1}$ and $\bar{3}$ in the IH, and the neutrino states 2 and 3 in the NH. In both cases the effect is seen most strongly for the higher energies since the density profile lingers in the H resonance region corresponding to the higher neutrino energies. Additionally, at the lowest energies we see that neutrino states 1 and 2 are affected by the MSW L resonance since it has become diabatic with the turbulence induced resonances. A strong phase effect from the multiple resonances is visible in all the affected channels.

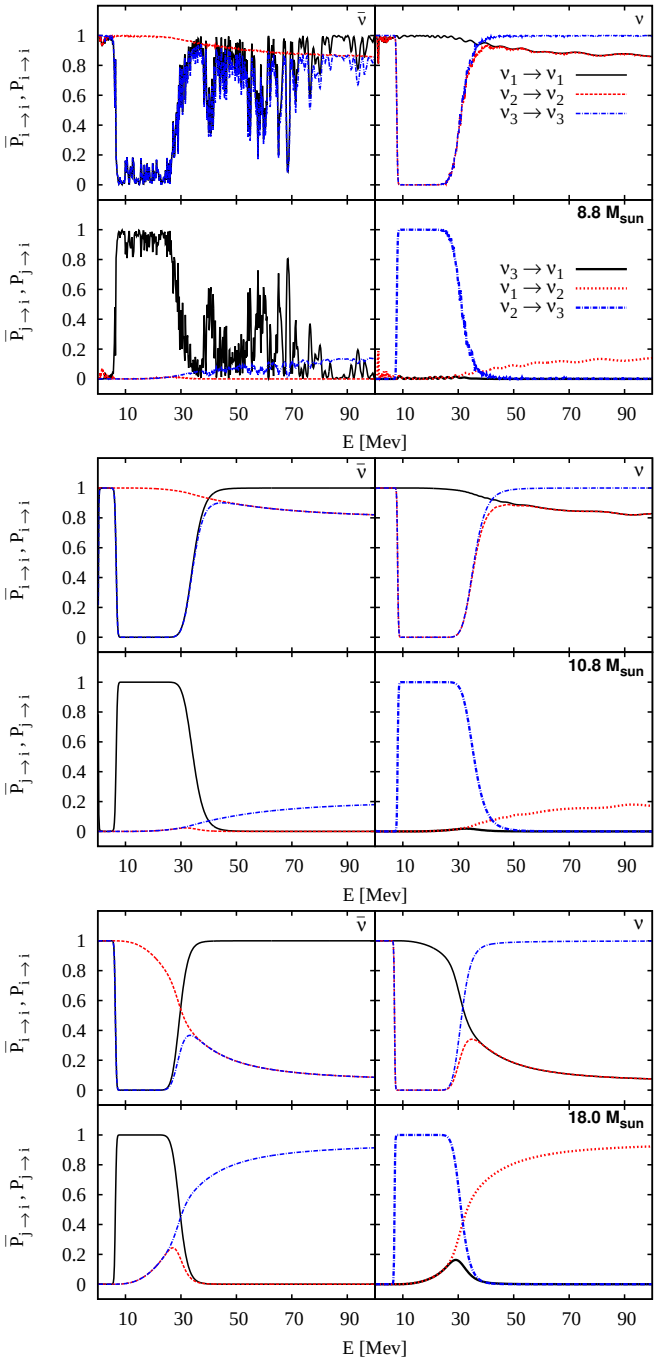

FIG. 20. (color online). As Fig. 16 but for the full profile traversal with 10% turbulence. Inverted Hierarchy.

IV. TIME EVOLUTION OF FEATURES

In Sections III A and III B we saw how features in the neutrino survival probabilities arose and subsided as time progressed. We saw how the self-interaction induced dou-

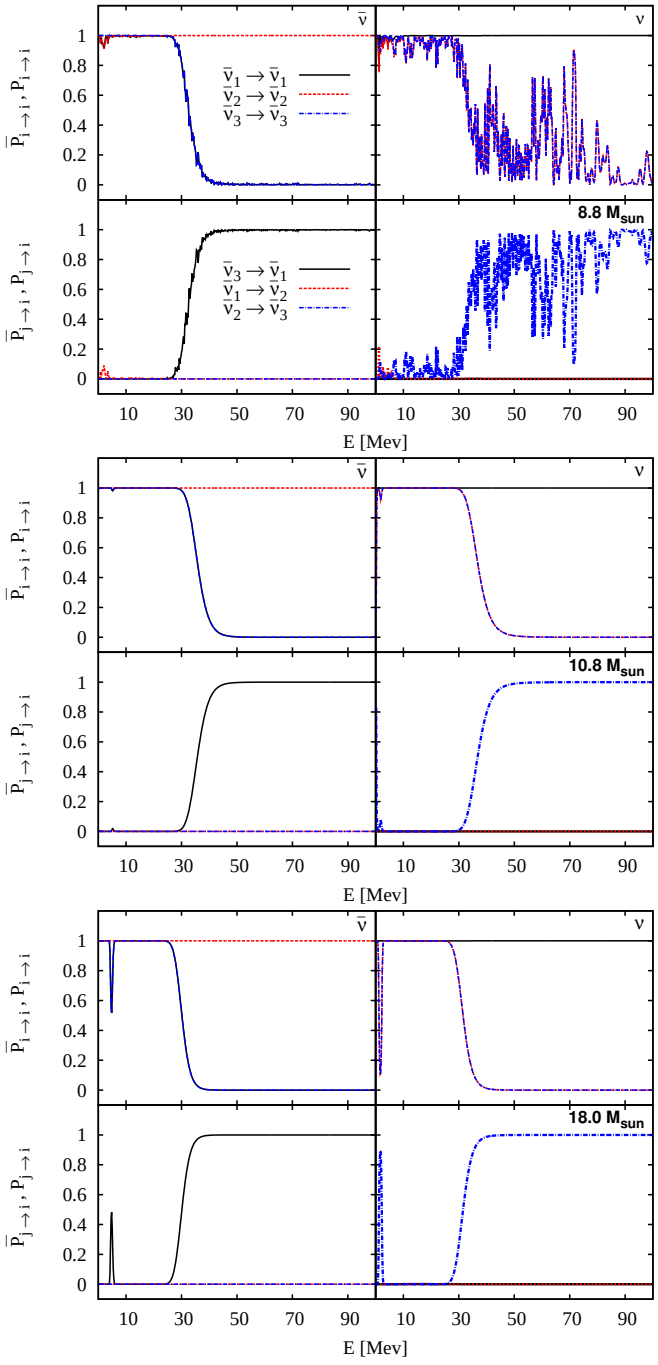

FIG. 21. (color online). As Fig. 17 but for the full profile traversal with 10% turbulence. Normal Hierarchy.

ble split between neutrino states 2 and 3 in the IH grew more narrow from 1 s to 3 s because the higher energy spectral split moved down in energy. Similarly we saw in the NH that the self-interaction splits between states $\bar{1}$ and $\bar{3}$, and between states 2 and 3 also moved down in energy. Hardly any imprint of the MSW effect was present at 1 s thus it is hard to discuss the evolution of MSW imprints from the 1 and 3 s profiles alone. However, as will become apparent below, the MSW imprints evolve significantly when we look at later times.

If observed, one might hope that such time dependence of the features imposed by both neutrino self-interactions and the MSW effect (as well as turbulence) will lead to a better handle on and understanding of the neutrino flavor evolution. In this section we therefore more thoroughly discuss the time evolution of some collective and MSW induced features. The movement in energy of both the shock-induced and the collective-induced spectral splits is associated with the evolution of the density profiles. As time passes the shock front moves progressively further out, and thus into lower density regions, bringing higher energy neutrinos into resonance, see Figures 22 and 23. The MSW shock-induced spectral splits therefore move up in energy. The self-interaction induced splits change due to the decreasing neutrino density close to the PNS, allowing less and less time for collective oscillations to develop. Additionally the neutrino luminosities and mean energies decrease over the same time frame causing the interaction strength to diminish.

All these changes to the density profiles, neutrino luminosities and mean energies lead to a complicated evolution of the flavor evolution that one would hope to disentangle from a real neutrino burst signal. From a careful analysis of which effects create which features we shall see that the time evolution of MSW collective effect signatures is unique. We will focus first on the time evolution of the probabilities that are caused by the progression of the shock front, then we will discuss the time evolution of a sample feature of the collective effect.

A. Progression of the shock front and its impact on probabilities

The shock wave features in the signal are inserted in the outer region of the supernova envelope therefore we focus upon this region exclusively for the time being. In-

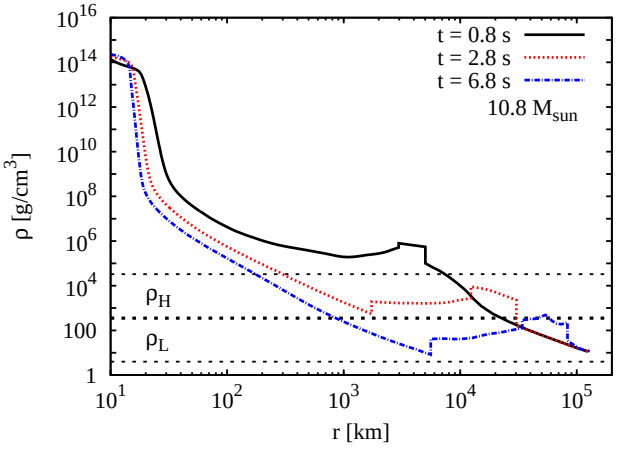

FIG. 22. (color online). Density profiles at 3 different times for our 10.8 $M_\odot$ model.

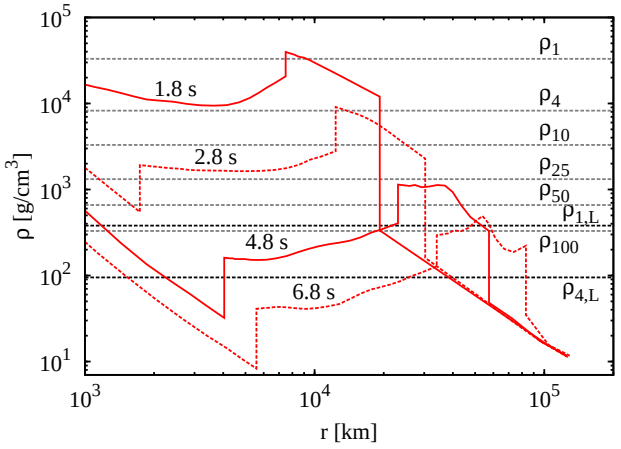

FIG. 23. (color online). Density profiles for the 10.8 $M_\odot$ model showing the progression of the forward shock through resonant density layers. The neutrino energy corresponding to a given resonance is given in MeV. The resonant densities are calculated with the assumption $Y_e = 0.5$.

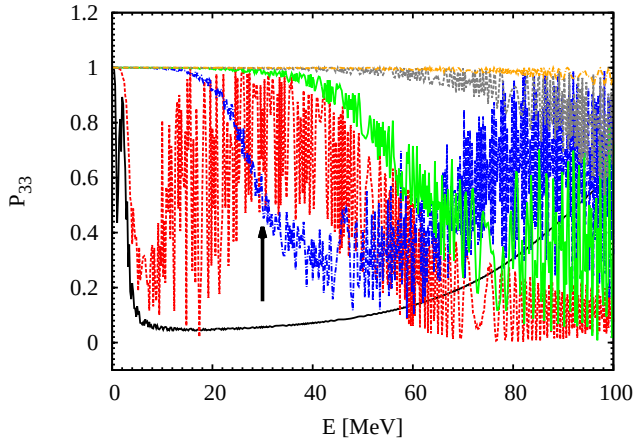

FIG. 24. (color online). Survival probabilities for neutrino matter state 3, P_{33}, at 1.8 s (black solid line), 2.8 s (red dashed line), 4.8 s (blue dot-dashed line), 5.8 s (green solid line), 6.8 s (gray dashed line) and 7.8 s (yellow dot-dashed line) for our 10.8 $M_\odot$ model in the NH and for the outer regions. The black arrow at 30 MeV marks on the 4.8 s profile the drop from unit survival probability discussed in the text.

cluding the collective effects from the inner region would make the probabilities more complex and make it harder to show the effects we are trying to illustrate. Narrowing our focus further we shall consider the 10.8 $M_\odot$ model and the NH where the effect of the MSW H (high density) resonance is to mix neutrino matter states 2 and 3. We shall discuss the evolution of the other two models later. In Fig. 24 we show the survival probability of neutrino matter state 3 for several different times. We will not consider the survival probability of matter state 2 since it is also entangled with the survival probability of matter state 1 through the MSW L (low density) resonance. Multiple features in the P_{33} survival probabilities in Fig. 24 deserve attention and further explanation. First and foremost we would like the reader to focus on the drop from unit survival probability which occurs at all times, but which appears at low energies for early times and progresses to higher energies at later times. In Fig. 24 we have indicated with a black arrow on the $t = 4.8s$ result (blue dot-dashed line) the drop feature in question. We see that the midpoint of the drop moves from about 4 MeV at 2.8 s, to 25 MeV at 4.8 s, to 56 MeV at 5.8 s. At 6.8 s the shock is beginning to slip out of the energy range we consider and by 7.8 s it has vanished. The probability drop from $P = 1$ to $P \sim 0$ has a direct relation to the appearance of the density profile. For the sake of clarity we have selected a small sample of the density profiles we are investigating and show them in Fig. 23. This figure illustrates the progression of the forward shock through the MSW H resonance region, and we clearly see how the forward shock moves out and into lower densities, thereby changing the resonance of the neutrinos with higher and higher energies from adiabatic to diabatic. If the shock feature can be found and followed in the neutrino signal then it should be possible to map that back so as to follow the progression of the shock front over time through the star.

The probability P_{33} at 1.8 s (black solid line in Fig. 24) shows a particularly interesting feature at energies below 5 MeV: a double drop. From the corresponding density profile in Fig. 23 we see that the contact discontinuity at this particular snapshot of the simulation covers resonant densities corresponding to energies of 1–2 MeV and the forward shock covers energies of 3–100 MeV. This leaves a tiny gap of roughly an MeV in which the neutrino transition probability is not enhanced. This is reflected in the probability in Fig. 24 where we see an initial drop in survival probability at 1–2 MeV, followed by an increase in the survival probability around 3 MeV, only to drop again at 4 MeV. Part of the reason the initial drop and the subsequent increase in survival probability is incomplete is that the flavor conversion resonances have widths which are proportional to $\tan 2\theta$. Another manifestation of this effect is the gradual change from a survival probability of 1 to 0 over a range of energies, as can be seen e.g. in the $t = 4.8s$ result (blue dot-dashed line) where the drop occurs over energies of $\sim$ 12–44 MeV. The rapid oscillations in energy that overlay the large scale trends mentioned above is caused by phase effects, which we have discussed before.

We now take a closer look at the survival probability P_{33} for the 2.8 s profile with its multitude of features, and investigate how they relate to features in the corresponding density profile. From Fig. 23 we clearly see the discontinuous jump, that is the reverse shock, spans densities corresponding to the resonant densities for neutrinos with energies between 17 and 62 MeV. Similarly the contact discontinuity spans densities corresponding to energies in the range 3.5 to 12 MeV and the forward shock covers energies from about 14 to 210 MeV. Con-

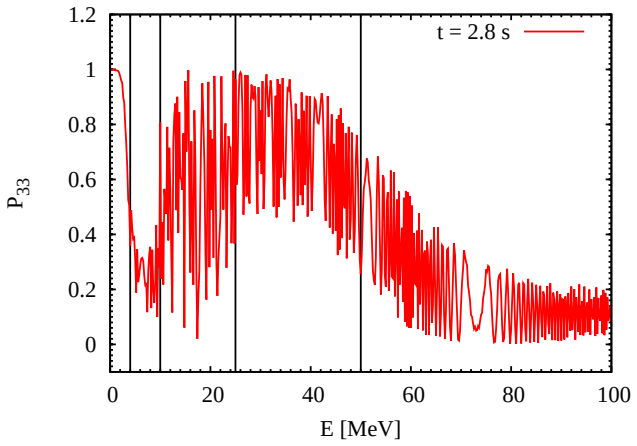

FIG. 25. (color online). Survival probability for neutrino matter state 3, P_{33}, at 2.8 s for our 10.8 $M_\odot$ model (red solid line) in the NH and for the outer region. The vertical lines are the energies for which the H resonant densities are marked in Fig. 23 (gray dashed lines).

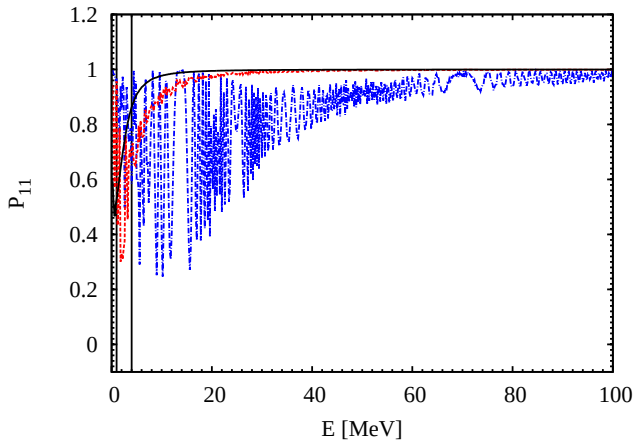

FIG. 26. (color online). Survival probability for neutrino matter state 1, P_{11}, at 1.8 s (black solid line), 2.8 s (red dashed line) and 4.8 s (blue dot-dashed line) for our 10.8 $M_\odot$ model in the NH and for the outer region. The vertical lines are the energies for which the L resonant densities are marked in Fig. 23 (black dashed lines).

sequently, a neutrino with an energy in one of the following ranges 3.5–12 MeV, 14–17 MeV or 62–210 MeV will only experience one diabatic resonant enhancement of its flavor conversion. If the neutrino instead possesses an energy in the range 17–62 MeV then it will experience two diabatic resonances; first at the reverse shock and secondly at the forward shock as it gets further out. A neutrino with an energy outside of these ranges will not experience any diabatic enhancement in the conversion probability. Neutrinos of all energies, outside the range 62 to 210 MeV, will also experience at least one adiabatic density resonance.

If we now turn our attention to Fig. 25, we see these features of the density profile reflected in the resonance survival probability P_{33}. The initial drop in survival probability at 3.5 MeV is caused by the diabatic crossing of the contact discontinuity enhancing the conversion of matter state 3 into matter state 2. Above 62 MeV we find the same familiar approach of P_{33} to 0 caused by a single diabatic resonance, this time due to the forward shock. The closely spaced energy regions of zero and single resonance between 12 and 14 MeV, and 14 and 17 MeV do not show their respective absent or full conversion due to the width of the resonances, which causes them to overlap. Neutrinos with energies between 17 and 62 MeV have two diabatic resonances due to the reverse and forward shocks, and in addition they can have up to 3 adiabatic resonances. The crossing of the reverse shock will enhance the conversion of matter state 3 into 2 and the subsequent passage of the forward shock will cause the neutrinos in matter state 2 to be converted back into matter state 3, leaving the survival probability at almost unity.

Consulting Fig. 26 allows us to determine that we expect a minimal impact from the L resonance. Fig. 26 show the survival probability of matter state 1 (which mixes with matter state 2 at the L resonance). From Fig. 23 we expect neutrinos with energies up to 2.5 MeV to be affected by a diabatic L resonance caused by the forward shock. Due to the width of the resonance actually neutrinos with up to about 24 MeV will feel the impact of the L resonance (see the red dashed line in Fig. 26). At energies above ∼17 MeV we see that 96% or more of the neutrino state 1 remain in state 1, while the remaining 4% or less mix with state 2. We can therefore conclude that the majority of neutrinos converted from matter state 3 into matter state 2 at the reverse shock H resonance will be converted back into matter state 3 at the forward shock. Although the majority of the neutrinos in matter state 2 remain in matter state 2, the small mixing with matter state 1 through the L resonance actually means we can have a tiny admixture of matter state 1 into matter state 3 (coming through matter state 2). Thus, this little example shows that it is not possible to completely separate the effect of the H and the L resonances, although the contamination is limited.

On top of the general undulating trend displayed in P_{33} – the initial drop around 3.5 MeV, the increase around 10 MeV and the subsequent slow fall off from roughly 40 to 60 MeV – we also see high frequency oscillations. These rapid oscillations are attributed to the phase effect. Phase effects arise when neutrinos encounters multiple resonances (diabatic or adiabatic) [90, 91]. Neutrinos of different energies will have slightly different path lengths between their respective resonance points so the phase will not be the same for each. Obviously the presence of the phase effects will make identifying shock-induced split features more difficult but the reader must be aware that the phase effects typically have such high "frequency" - "periods" of 50 keV or smaller - that current detectors are not capable of detecting them due to

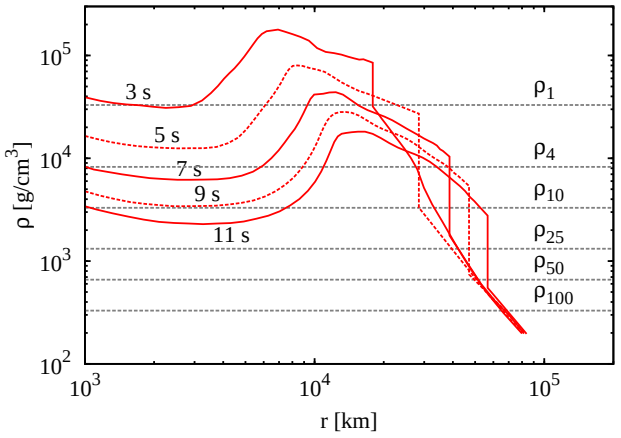

FIG. 27. (color online). Density profiles for the 18.0 $M_\odot$ model showing the progression of the forward shock through the MSW H resonant density layers. The horizontal gray dashed lines mark the resonant density for a neutrino of a given energy (in MeV).

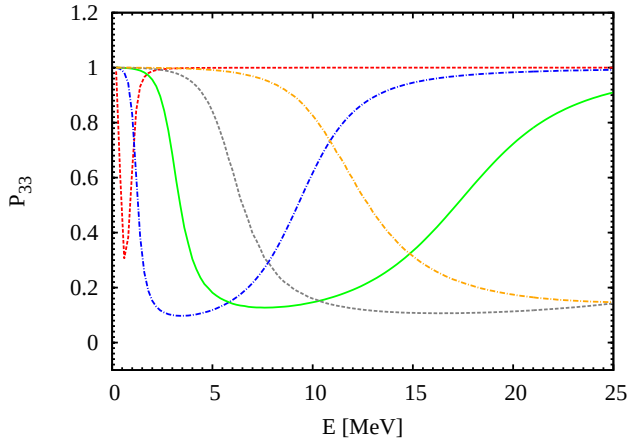

FIG. 28. (color online). Survival probabilities for neutrino matter state 3, P_{33}, at 3 s (red dashed line), 5 s (blue dot-dashed line), 7 s (green solid line), 9 s (gray dashed line) and 11 s (yellow dot-dashed line) for our 18.0 $M_\odot$ model in the NH and for the outer regions.

their comparatively lower energy resolution.

The connection between features of the density profile and features in the survival probabilities is readily made for all our profiles. We chose to focus on the 3 s profile of the the 10.8 $M_\odot$ model in this section because this profile possesses all three features in the density profile. Although not shown here, we see the exact same shock induced behavior in the anti-neutrino state $\bar{3}$ in case of the IH, and P_{11} exhibit a similar behavior in both hierarchies too. When we consider the other models we again find a match between profile features, and their evolution, and transition probability behavior. In the case of the 8.8 $M_\odot$ model the shock moves out so fast that our relative coarse sampling in time cannot follow it.

For the 18.0 $M_\odot$ model we see the effect of the progression of the shock wave almost as well as we do in the 10.8 $M_\odot$ case, see Figures 27 and 28. The major difference between the 10.8 $M_\odot$ and 18.0 $M_\odot$ models is not that the outward motion of the shock in the 18.0 $M_\odot$ progenitor is slightly slower than the shock progression in the 10.8 $M_\odot$ progenitor, they have similar speeds, but rather the profile of the 18.0 $M_\odot$ is so extended that the the shock feature of the transition probabilities takes much longer to sweep through the spectrum. For the survival probability P_{33} in Fig. 24, we followed the impact of the shock progression as the drop from $P = 1$ to $P \sim 0$ moved quickly from a few MeV through the entire spectrum and above 100 MeV in a handful of seconds (basically from 2 to 8 seconds). In contrast, in Fig. 28 we see how this same drop in P_{33} for the 18.0 $M_\odot$ model inches its way up through the energies; from below 1 MeV at 3 s to 12 MeV at 11 s. (Note the energy scale in Fig. 28 ends at 25 MeV not 100 MeV.) In addition to the much slower progression of the shock feature, the 18.0 $M_\odot$ model develops neither a contact discontinuity nor a reverse shock at the times we are looking at, so the probability plot in Fig. 28 is much "cleaner" than Fig. 24 for the 10.8 $M_\odot$ model. This absence of multiple resonances leads to an absence of phase effects in the 18.0 $M_\odot$ case. Finally, for the 18.0 $M_\odot$ model any discussion regarding the shock front moving into the L resonant density region is obviously moot since the L resonance densities starts at around 380 g/cm^3 and from Fig. 27 it is clear that only the very last couple of points on the density profiles are in this regime, and that the shock does not reach such low densities at the times we investigate here.

This very different evolution of MSW signatures in our progenitors means that identifying the MSW contribution to the neutrino signal can be turned around to learn about the progenitor. If the simulations we have used in this paper are representative then we expect ONeMg supernovae neutrinos to be briefly affected by shock waves early in the signal while much more massive progenitors are affected only after a longer delay and then the effects persist for much longer if not all of the remaining burst. Identifying what kind of star exploded makes the comparison of observations of the supernova via neutrinos, gravitational waves and photons with a simulation easier in the sense that we can compare like with like.

B. Time evolution of collective features

We now consider the time evolution of a few of the collective features and again focus our attention for the time being on the 10.8 $M_\odot$ model. For this one progenitor we plot in Figures 29 and 30 the time evolution of $\bar{P}_{33}$ and P_{33} in the inner region for a select set of times. Fig. 30 shows how the spectral split for the NH anti-neutrino survival probability $\bar{P}_{33}$ initially starts at 36 MeV at 0.8 s (green solid line). Then it moves down in energy until 2.8 s (red dashed line) where it reaches 26 MeV only to

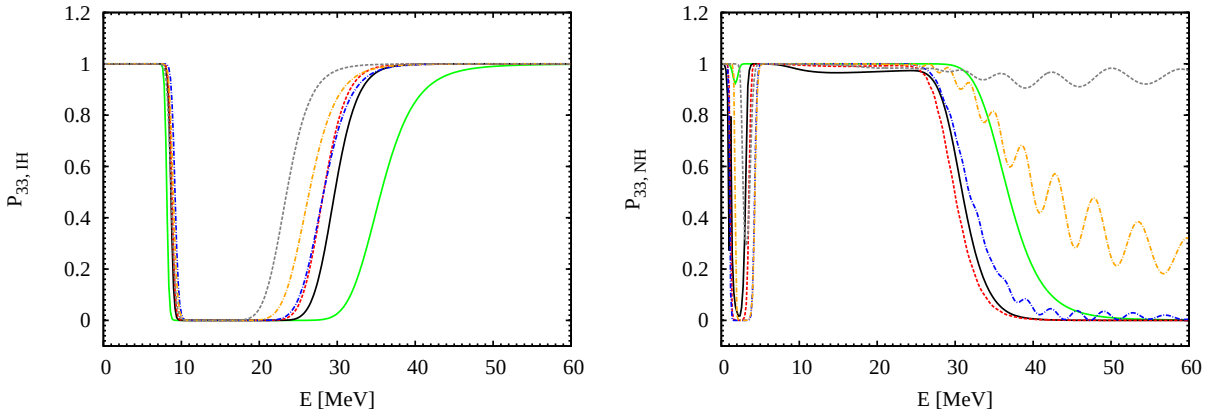

FIG. 29. (color online). Survival probabilities for neutrino matter state 3, P_{33}, at 0.8 s (green solid line), 1.8 s (black solid line), 2.8 s (red dashed line), 4.8 s (blue dot-dashed line), 7.8 s (yellow dot-dashed line) and 10.5 s (gray dashed line) for our 10.8 $M_\odot$ model for the inner regions. On the left for the IH and for the NH on the right.

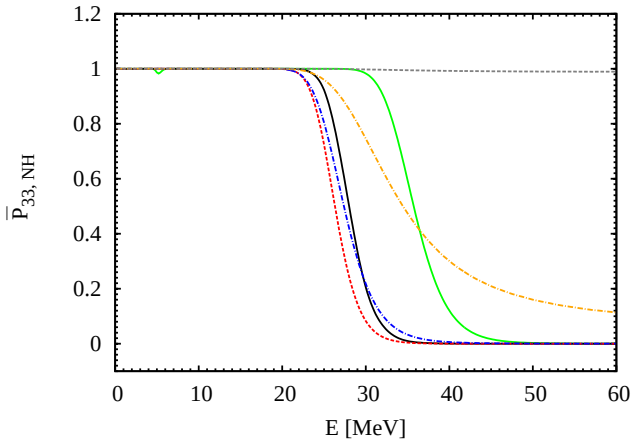

FIG. 30. (color online). Survival probabilities for anti-neutrino state $\bar{3}$, $\bar{P}_{33}$, at 0.8 s (green solid line), 1.8 s (black solid line), 2.8 s (red dashed line), 4.8 s (blue dot-dashed line), 7.8 s (yellow dot-dashed line) and 10.5 s (gray dashed line) for our 10.8 $M_\odot$ model for the inner regions and the NH.

climb back up in energy and become increasingly softer until the split is completely gone at 10.5 s (gray dashed line). Equally clean is the narrowing over time of the double spectral split in P_{33} in the IH that is shown in the left panel of Fig. 29. The higher energy split starts at 35.5 MeV at 0.8 s (green solid line) and gradually becomes steeper as it moves down in energy to end at 23.5 MeV at 10.5 s (gray dashed line). On the same time scale the spectral split at the lower energy starts at 8 MeV at 0.8 s, moves up to 9.2 MeV at 4.8 s, and then back down to 8.7 MeV at 10.5 s.

The evolution of P_{33} in the NH shown in the right panel of Fig. 29 is more convoluted. In this case, initially at 0.8 s (green solid line) there is only one split at an energy of 37 MeV, and a minuscule dip in the survival probability at 2 MeV. As time passes the higher energy split moves slightly down in energy until 2.8 s (red dashed line) where after it reverse direction and moves up in energy, becoming increasingly softer until it has almost disappeared at 10.5 s (gray dashed line). This is exactly as we saw in the anti-neutrino case but now we also observe at the later times oscillations in the survival probability. Meanwhile, at lower energies the initial dip at 2–3 MeV grows to a full double split feature that initially widens slightly and moves up in energy only to grow narrower again at late times. In principle one would expect to see this additional double spectral split arise over time in an observation. However, the two splits around 3 MeV are so closely spaced that current detector technology would not be able to resolve them, especially at such a low energy. By comparing the right panel of Fig. 29 to Fig. 24 we see that the energy range over which the probability features changes for the inner region is the same as the energy range for the outer region changes. Thus in an observed signal it would be a challenge if not impossible to disentangle the evolution from the two regions, let alone their time evolution.

The basic conclusion from these figures is that the collective features in any signal are not static but rather evolve in a fashion that does not lend itself to an easy analysis. Spectral splits due to collective effects can disappear over time and new ones at different energies emerge.

C. Late time evolution of the 10.8 $M_\odot$ and 18.0 $M_\odot$ models

In the previous subsections we investigated the detailed time evolution of important MSW and collective features separately. In this section we will show the combined probabilities for a (anti-)neutrino traversing the full profile. We show the survival probabilities in both hierarchies for three late time profiles of the 10.8 $M_\odot$ and

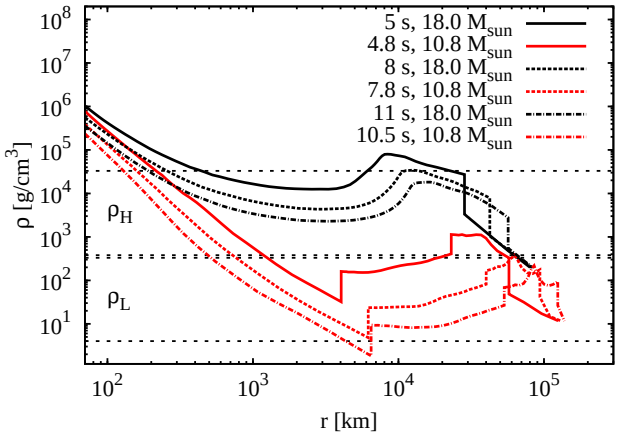

FIG. 31. (color online). Density profiles for the 10.8 $M_\odot$ progenitor at 4.8 s (solid red), 7.8 s (dashed red) and 10.5 s (dot-dashed red), as well as for the 18.0 $M_\odot$ progenitor at 5 s (solid black), 8 s (dashed black) and 11 s (dot-dashed black).

18.0 $M_\odot$ progenitors in Figures 32 and 33 respectively. For the 10.8 $M_\odot$ progenitor we show results at 4.8 s (top quartets), 7.8 s (middle quartets) and 10.5 s (bottom quartets). The corresponding density profiles are shown in Fig. 31 (red lines) along with the appropriate density profiles for the 18.0 $M_\odot$ model (black lines). Fig. 33 show the results at 5 s (top quartets), 8 s (middle quartets) and 11 s (bottom quartets) for the 18.0 $M_\odot$ progenitor. The complete simulation of the 18.0 $M_\odot$ model runs to a post bounce time of 21.4 seconds, and going into a meticulous discussion would require almost a paper on its own. Fortunately the evolution of the density profile over the last 10 s is rather limited, thus we show only a couple of examples of the late time results in Fig. 33.

The two progenitors have several features in common, and a few differences that can easily be related back to the behavior of their respective density profiles. The most obvious feature displayed by the two progenitor's probabilities is the collective-induced double split in the IH for neutrino states 2 and 3 (right panels of the left most quartets in Figures 32 and 33), that was discussed at length above. Equally clear is the spectral split in the anti-neutrino states $\bar{1}$ and $\bar{3}$ in the NH (left panels of the right most quartets in Figures 32 and 33). This split is present in both progenitors at the two earlier snapshots, and then it has disappeared by the last snapshot at ∼11 s. The time evolution of this split was discussed previously for the 10.8 $M_\odot$. These two very prominent collective features are in sharp contrast to the absence of collective features in anti-neutrinos in the IH, occurring in both progenitors. A slightly curious result of this investigation is the time duration over which the collective features remain visible. One would expect the collective features to disappear from the probabilities as the interaction strength diminishes over time with the decreasing density. We mentioned in Sec. IV B that there is no analytical way of predicting the exact evolution of collective features from the current understanding of neutrino self-interactions. However, based on Fig. 31 it would appear plausible that the largest effect of self-interaction takes place within the first ∼150–200 km where the densities remain on the same order as time progresses. Thereby resulting in similar collective features over time and across progenitors.

For both progenitors the behavior of the collective features in neutrino states 2 and 3 in the NH is significantly tangled with the evolution of the MSW features in the same energy region (right panels of the right most quartets in Figures 32 and 33). We alluded to this fact towards the end of the previous subsection. This entangled behavior of collective and MSW features leads us to some of the features that differ between the two progenitors. Unsurprisingly these features are dominantly MSW induced, and easily related back to the differences in the density profiles.

The underlying collective features in neutrino states 2 and 3 in the NH are two sharp spectral splits at 2 and 4 MeV, and a slightly softer spectral split at ∼30 MeV. The MSW then adds a "shock" feature, very similar to the one seen in the IH anti-neutrino states $\bar{1}$ and $\bar{3}$ for the 18.0 $M_\odot$, to the probabilities. Tackling one progenitor at the time, we'll start with the 10.8 $M_\odot$ model: The two low energy collective splits are visible throughout the times we are examining although they are clearly in the process of vanishing at 10.5 s. The MSW effect of the contact discontinuity at 4.8 s is to generate a "shock"-induced split for neutrinos with energies above ∼30 MeV (cf. Fig. 23). This "shock"-induced split is overlapping in energy with the collective swap also around 30 MeV. Therefore we see an initial decline in the survival probabilities P_{22} and P_{33} prior to 30 MeV, followed by a swap back to nearly unit survival probability just after 30 MeV. At 7.8 s the contact discontinuity has moved out of the H resonance region, and the corresponding "shock"-induced split just below ∼30 MeV in neutrino states 2 and 3 have gone, leaving only the collective split at 30 MeV before that too is gone by 10.5 s.

Moving to the 18.0 $M_\odot$ progenitor we see a similar story, only without any obscuring phase effects as the 18.0 $M_\odot$ develops only a forward shock. As with the 10.8 $M_\odot$ model the underlying collective effects in neutrino states 2 and 3 in the NH (left panels of the right most quartets of Fig. 33) are two spectral splits at 2 and 4 MeV, with an additional split at 30 MeV. In this case however the MSW effect is caused by the forward shock. At 5 s the forward shock is affecting neutrinos of energies from roughly 1 to 10 MeV, whereas the affected neutrinos have energies of 10 to roughly 60 MeV at 11 s (cf. Fig. 27). By 11 sec the collective interaction have subsided so much that the split at 30 MeV has vanished. A remnant of the low energy double split remains, but the main flavor conversion is induced by the MSW effect due to the forward shock. At 5 s initially the collective effect causes the swap of neutrinos with energies between

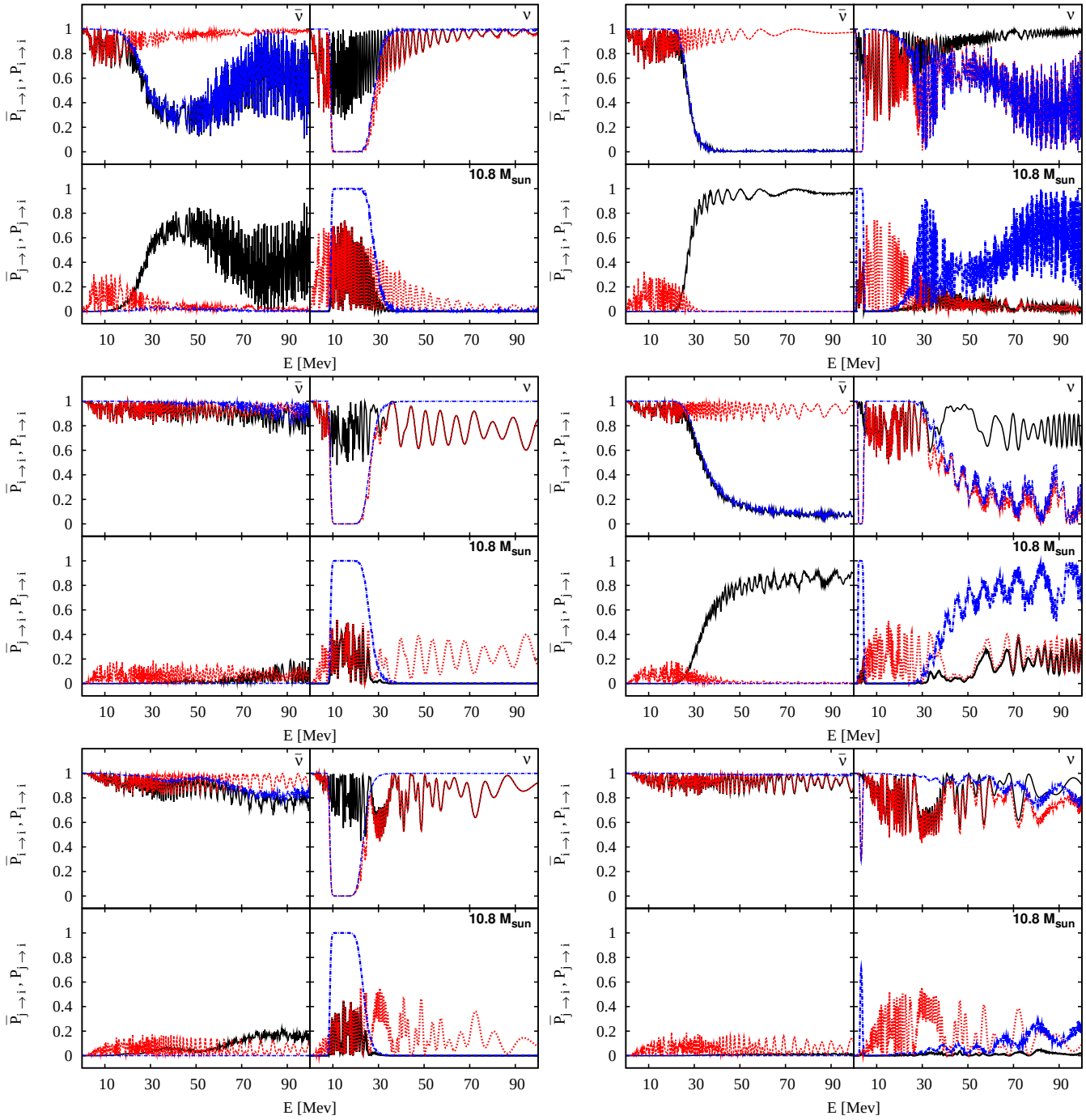

FIG. 32. (color online). Matter survival and transition probabilities for the 10.8 $M_\odot$ model. All results are for a full profile calculation. Top to bottom quartets have probabilities from 4.8 s, 7.8 s and 10.5 s. On the left side is the IH and on the right side is the NH. Each quartet has the same layout as the middle quartet of Fig. 10 and line styles have the same meaning.

2 and 4 MeV. Then the shock feature arises and forces neutrinos with energies already from 1 MeV to swap, but when the shock impacts the already swapped neutrinos in the energy region 2–4 MeV it swaps them back, making their survival probability approach unity. The forward shock continues to affect neutrinos with energies up to ∼10 MeV causing the drop in the survival probabilities P_{22} and P_{33} below 10 MeV. At 8 s the impact of the forward shock is on neutrinos with energies between 4 and ∼29 MeV. We see how this causes the survival probabilities to drop in between the self-interaction induced splits at 4 and 30 MeV.

The remaining MSW features are quickly summarized and explained: A swap in the anti-neutrino states $\bar{1}$ and

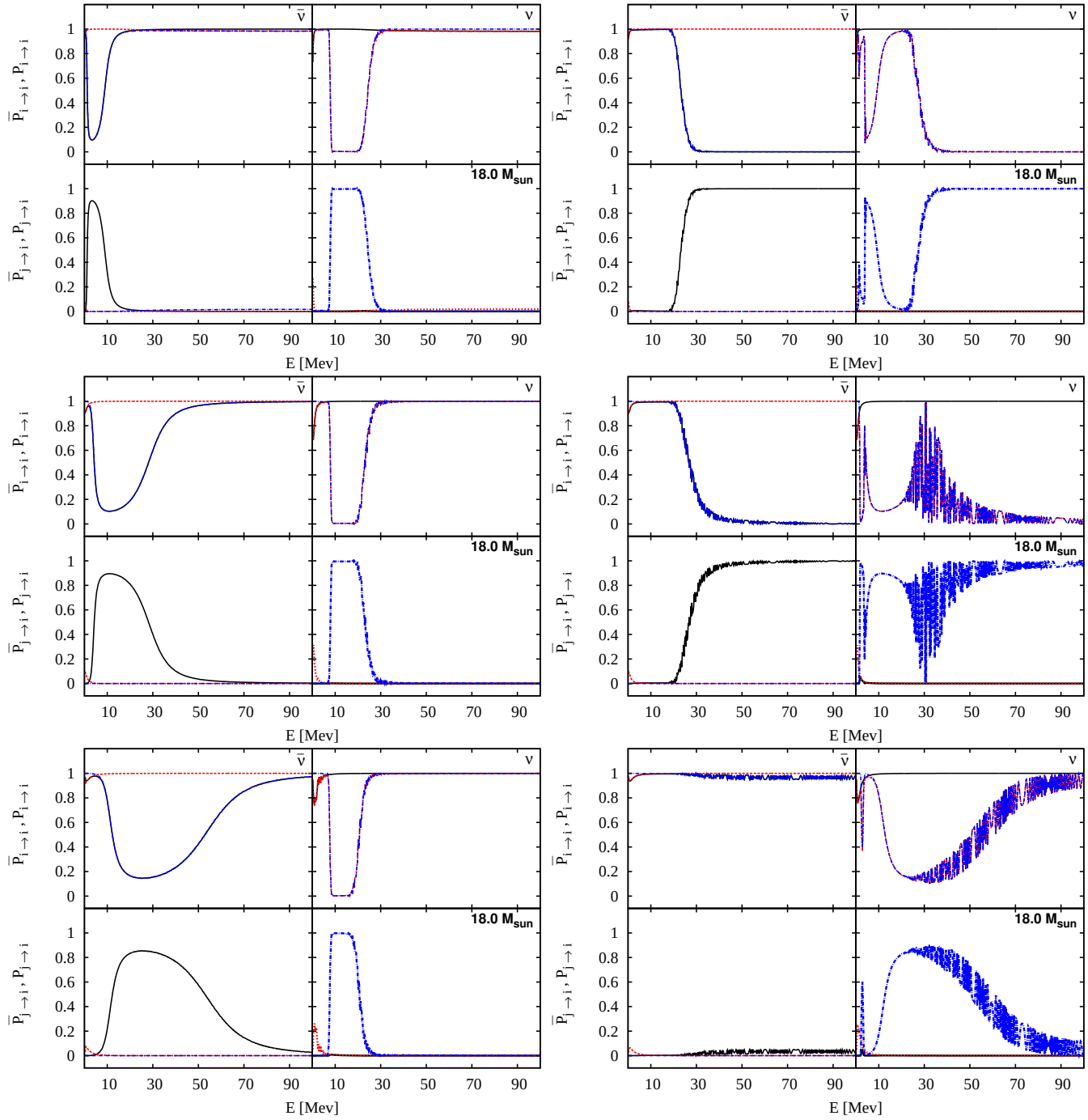

FIG. 33. (color online). As in Fig. 32, but for the 18.0 $M_\odot$ model. From top to bottom the quartets are at 5 s, 8 s and 11 s. Left side is the IH and the right side is the NH.

$\bar{3}$ in the IH of the intermediate and higher energy neutrinos in the 10.8 $M_\odot$ progenitor is caused by the diabatic contact discontinuity. By 7.8 s all features in the density profile of the 10.8 $M_\odot$ model have moved out of the H resonance region and into the L resonance region. This is reflected in the survival probabilities for neutrino states 1 and 2 in both hierarchies, as they drop from unity at low and intermediate energies. The multiple diabatic resonances caused by the contact discontinuity, reverse and forward shocks (visible in Fig. 31) lead to dominating phase effects.

In the 18.0 $M_\odot$ progenitor the forward shock, although moving to higher energy resonant densities, remains in the H resonance region (black lines in Fig. 31). The impact of this was already mentioned above for neutrino states 2 and 3 in the NH, and is plainly visible in anti-

neutrino states $\bar{1}$ and $\bar{3}$ in the IH too. Although the shock itself does not reach into the L resonant densities the width of the L resonance causes a small mixing of neutrino states 1 and 2 at very low energies, an effect visible in both hierarchies of the 8 s and the 11 s results.

V. CONCLUSIONS

In this paper we have aimed at uncovering the rich phenomenology that arises in the neutrino spectra from the combination of self-interactions, MSW interactions and turbulence in core-collapse supernovae. We have calculated the neutrino flavor evolution through realistic density profiles from 1D numerical simulations and found that the signal can, potentially, provide great insight into what takes place inside a core-collapse supernova, but that insight comes at a price. The various flavor transformation processes leave complex features that depend sensitively on a wealth of quantities: the detailed ratios of energies and luminosities between neutrino flavors, the density profile of the progenitor star and its time development especially with respect to shocks and turbulence, and the magnitude of the turbulence. Many of these aspects have been investigated separately hitherto, but from the investigation presented here, it is clear that for a comprehensive picture one needs to tackle all of these effects together.

We have calculated the flavor conversion caused by collective, MSW and turbulence effects separately and in combination as neutrinos leave a core-collapse supernova. We find that the self-interaction induced spectral splits are similar at equal times for all three progenitor masses investigated here. The similarities can be ascribed to two factors: The ratio between the number fluxes of the different neutrino flavors are almost identical for the three progenitors, and the differences between the matter density profiles inside 1000 km are only moderate, indicating that the neutrino densities are somewhat similar. We have pointed out several prominent features in the survival probabilities that persist and evolve over time. These include spectral splits in both hierarchies for both neutrinos and anti-neutrinos, and are consistent with previous findings, albeit different in detail.

Moving further out into the supernova mantle we have found that the impact of MSW effects are significant only at later times, and that of our three progenitors the 10.8 $M_\odot$ model shows the largest effects in the neutrino survival probabilities. We have shown how one can in principle follow the progression of the shock front in the star by following how the shock-induced spectral split related to the MSW H resonance moves in energy. We have shown how this shock feature moves rapidly over almost two orders of magnitude in energy for the 10.8 $M_\odot$ model, but only over an order in energy for the 18.0 $M_\odot$ model. Should it be possible to identify this shock feature in a future observation of neutrinos from a galactic supernova, it could potentially give us a hint about the progenitor mass. For the 10.8 $M_\odot$ progenitor we were furthermore able to follow the shock front moving into the MSW L resonant density layers. As a consequence we can present, for the first time, results of calculations on how this resonance impacts the neutrino flavor probabilities. We found the anticipated conversions between neutrino matter states 1 and 2, and found them to have approximately the same magnitude in both hierarchies as expected due to the largeness of θ_{12}.

Through calculations combining both collective interactions and MSW interactions we have shown that the net effect can lead to a wash out of features that would be expected from treating the two effects separately. The subsequent influence of the MSW interaction will (partially) undo the impact of the self-interaction. Consequently future investigations should include both effects when predicting observable features.

We have shown that including moderate amounts of turbulence has a limited effect on the flavor evolution for the two heaviest progenitors. On the lightest progenitor the impact of turbulence hinges sensitively on the instantaneous density profile. Over a few seconds the impact of turbulence goes from moderately significant at 1 s to non-existent at 3 s. Increasing the amplitude of turbulence we found that large amounts of turbulence can obscure features induced by the neutrino self-interactions or the MSW effect. This general conclusion holds for all of our three progenitors although in this paper we have only presented results from the 10.8 $M_\odot$ model. We find that the impact of large amounts of turbulence can be summarized as both obstructive and constructive. On the constructive side we find that large amounts of turbulence will lead to novel mixing phenomena in the anti-neutrino channel in the NH as discussed in Sec. III A 5. Furthermore, large turbulence leads to increased mixing between neutrino states 1 and 2 at low energies in both hierarchies. On the destructive side large amounts of turbulence will obscure some signal features.

We expect some of the spectral splits and large scale features in the neutrino probabilities will be observable in a future neutrino signal. Especially the NH neutrino split at $\sim$30 MeV between states 2 and 3 or the anti-neutrino split between states $\bar{1}$ and $\bar{3}$ around 25 MeV might be visible. In an upcoming paper [92] we will examine in more detail the prospect of observing some of the features described in this paper. However, presently it is clear that with the energy resolution of current detector technology the high frequency oscillations imposed on the survival probabilities by the phase effect will not be observable. For diagnostic purposes in a future observed neutrino signal we find that the NH generally always has a spectral split around 30 MeV in the neutrino sector and, in most snapshots, we also find a similar split around 25 MeV in the anti-neutrino sector. Both of these splits are induced by collective effects and appear to survive MSW effects and the addition of moderate amounts of turbulence, al-

though the neutrino split does not survive large turbulence. The spectra in the IH are much more dependent upon time but a persistent feature is the double spectral split in neutrinos at ∼8 MeV and 23–35 MeV. This feature is again induced by collective effects and survives the impact of the MSW interaction in the outer regions. Unlike the neutrino feature discussed above for the NH, this double split survives both the addition of moderate and large amounts of turbulence. The upper split is in an energy region where it is could actually be observed. However, this requires that future detectors focused on neutrinos are built, and with a large future neutrino detector to compliment current (and future) anti-neutrino detectors we may gain evidence for the hierarchy from an observation of spectral splits in a neutrino signal.

In order to decode a real neutrino burst signal from a Galactic supernova we cannot continue to investigate collective and MSW effects separately, but have to treat them in combination. With our upcoming paper predicting the observed signals, we aim to show how these features will appear in an observation and how we might use such observations to learn about the neutrino mass hierarchy, neutrino interactions in dense matter, the mechanism of core-collapse supernovae and potentially the progenitor mass.

ACKNOWLEDGMENTS

We acknowledge support by the Department of Energy under grant number DE-SC0006417. We gratefully acknowledge access to data from Tobias Fischer.

[1] Murphy, J. W., & Meakin, C., Astrophys. J.**742** 74 (2011)
[2] Ott, C. D., Abdikamalov, E., Moesta, P., et al., accepted to Astrophys. J.(2013) [arXiv:1210.6674]
[3] Dolence, J. C., Burrows, A., Murphy, J. W., & Nordhaus, J., (2012) [arXiv:1210.5241]
[4] Hanke, F., Marek, A., Müller, B., & Janka, H.-T., Astrophys. J.**755** 138 (2012)
[5] Pejcha, O., & Thompson, T. A., Astrophys. J.**746** 106 (2012)
[6] Müller, B., Janka, H.-T., & Heger, A., Astrophys. J.**761** 72 (2012)
[7] Takiwaki, T., Kotake, K., & Suwa, Y., Astrophys. J.**749** 98 (2012)
[8] Lentz, E. J., Bruenn, S. W., Harris, J. A., et al., arXiv:1301.1326 (2013) Proceedings of the "12th Symposium on Nuclei in the Cosmos." 2012.
[9] Y. Suwa, K. Kotake, T. Takiwaki, S. C. Whitehouse, M. Liebendoerfer and K. Sato, Publ. Astron. Soc. Jap. **62**, L49 (2010) [arXiv:0912.1157]
[10] Y. Suwa, K. Kotake, T. Takiwaki, M. Liebendorfer and K. Sato, Astrophys. J. **738**, 165 (2011) [arXiv:1106.5487]
[11] T. Fischer, S. C. Whitehouse, A. Mezzacappa, F.-K. Thielemann and M. Liebendörfer, A&A **517A**, 80F (2010) [arXiv:0908.1871v2].
[12] Müller, E. and Janka, H.-Th. and Wongwathanarat, A., A&A 537, A63 (2012) [arXiv:1106.6301]
[13] Nakazato, K., Sumiyoshi, K., Suzuki, H., Totani, T., Umeda, H. and Yamada, S., Astrophys. J. Supp. **205** 2 (2013) [arXiv:1210.6841]
[14] Hüdepohl, L., Müller, B., Janka, H.-T., Marek, A. and Raffelt, G.G., Phys. Rev. Lett.**104** 251101 (2010) [arXiv:0912.0260]
[15] Burrows, A., (2012) [arXiv:1210.4921]
[16] Janka, H.-Th., Ann. Rev. Nucl. Part. Sci. **62**, 407 (2012) [arXiv:1206.2503]
[17] M. Ugliano, H. T. Janka, A. Marek and A. Arcones, Astrophys. J. **757**, 69 (2012) [arXiv:1205.3657]
[18] C. D. Ott, A. Burrows, L. Dessart and E. Livne, Astrophys. J. **685**, 1069 (2008) [arXiv:0804.0239]
[19] S. W. Bruenn, A. Mezzacappa, W. R. Hix, E. J. Lentz, O. E. B. Messer, E. J. Lingerfelt, J. M. Blondin and E. Endeve *et al.*, Astrophys. J. Lett. **767**, L6 (2013) [arXiv:1212.1747].
[20] E. J. Lentz, A. Mezzacappa, O. E. Bronson Messer, W. R. Hix and S. W. Bruenn, Astrophys. J. **760**, 94 (2012) [arXiv:1206.1086]
[21] E. J. Lentz, A. Mezzacappa, O. E. Bronson Messer, M. Liebendorfer, W. R. Hix and S. W. Bruenn, Astrophys. J. **747**, 73 (2012) [arXiv:1112.3595]
[22] T. Kuroda, K. Kotake and T. Takiwaki, Astrophys. J. **755**, 11 (2012) [arXiv:1202.2487]
[23] O'Connor, E. and Ott, C. D., Astrophys.J.˜**762** 126 (2013) [arXiv:1207.1100]
[24] Scholberg, K. 2012, Annual Review of Nuclear and Particle Science, 62, 81
[25] Lund, T., Marek, A., Lunardini, C., Janka, H.-T., & Raffelt, G., Phys. Rev. D**82** 063007 (2010)
[26] Lund, T., Wongwathanarat, A., Janka, H.-T., Müller, E., & Raffelt, G., Phys. Rev. D**86** 105031 (2012)
[27] C. D. Ott, E. P. O'Connor, S. Gossan, E. Abdikamalov, U. C. T. Gamma and S. Drasco, Nucl. Phys. Proc. Suppl. **235-236**, 381 (2013) [arXiv:1212.4250]
[28] S. P. Mikheyev and A. I. Smirnov, Nuovo Cimento C **9** 17 (1986)
[29] L. Wolfenstein, Phys. Rev. D**17** 2369 (1978)
[30] Reid, G., Adams, J., & Seunarine, S., Phys. Rev. D**84** 085023 (2011)
[31] S. Choubey, B. Dasgupta, A. Dighe and A. Mirizzi, (2010) [arXiv:1008.0308v1]
[32] Fogli, G., Lisi, E., Marrone, A. & Tamborra, I., JCAP **0910** 002 (2009) [arXiv:0907.5115v2]
[33] Duan, H., Fuller, G. M., Carlson, J. and Qian, Y.-Z., Phys. Rev. D**74** 105014 (2006) [arXiv:astro-ph/0606616v2]
[34] J. T. Pantaleone, Phys. Lett. B **287**, 128 (1992).
[35] S. Samuel, Phys. Rev. D**48**, 1462 (1993).
[36] H. Duan, G. M. Fuller and Y. Z. Qian, Phys. Rev. D**74**, 123004 (2006)
[37] S. Pastor, G. G. Raffelt and D. V. Semikoz, Phys. Rev. D**65**, 053011 (2002)
[38] S. Hannestad, G. G. Raffelt, G. Sigl and Y. Y. Y. Wong, Phys. Rev. D**74**, 105010 (2006) [Erratum-ibid. D **76**, 029901 (2007)]
[39] G. G. Raffelt and A. Y. Smirnov, Phys. Rev. D**76**, 081301 (2007) [Erratum-ibid. D **77**, 029903 (2008)]
[40] Raffelt, G. G., Phys. Rev. D**78** 125015 (2008)
[41] Mirizzi, A., & Serpico, P. D., Phys. Rev. Lett.**108** 231102 (2012)
[42] Mirizzi, A., & Serpico, P. D., Phys. Rev. D**86** 085010 (2012) [arXiv:1208.0157]
[43] Cherry, J. F., Carlson, J., Friedland, A., Fuller, G. M., & Vlasenko, A., Phys. Rev. Lett.**108** 261104 (2012)
[44] A. Friedland, Phys. Rev. Lett. **104** 191102 (2010) [arXiv:1001.0996v2]
[45] B. Dasgupta, A. Mirizzi, I. Tamborra and R. Tomás, Phys. Rev. D **81**, 093008 (2010) [arXiv:1002.2943v2]
[46] H. Duan and A. Friedland, Phys. Rev. Lett. **106** 091101 (2011) [arXiv:1006.2359]
[47] Galais, S., Kneller, J., & Volpe, C., Journal of Physics G Nuclear Physics, **39** 035201 (2012)
[48] Chakraborty, S., Fischer, T., Mirizzi, A., Saviano, N., & Tomàs, R., Phys. Rev. Lett.**107** 151101 (2011)
[49] Sarikas, S., Tamborra, I., Raffelt, G., Hüdepohl, L., & Janka, H.-T., Phys. Rev. D**85** 113007 (2012)
[50] R. C. Schirato and G. M. Fuller, arXiv:astro-ph/0205390.
[51] Roberts, L.F., Reddy, S. and Shen, G., Phys. Rev. C **86** 065803 (2012) [arXiv:1205.4066]
[52] Horowitz, C.J., Shen, G., O'Connor, E. and Ott, C. D., Phys. Rev. C **86** 065806 (2012) [arXiv:1209.3173]
[53] Reddy, S., Prakash, M. and Lattimer, J. M., Phys. Rev. D**58** 013009 (1998) [arXiv:astro-ph/9710115]
[54] Martínez-Pinedo, G., Fischer, T., Lohs, A. and Huther, L., Phys. Rev. Lett. **109** 251104 (2012) [arXiv:1205.2793]
[55] J. F. Cherry, J. Carlson, A. Friedland, G. M. Fuller and A. Vlasenko, (2013) [arXiv:1302.1159]
[56] Banerjee, A., Dighe, A. and Raffelt, G. Phys. Rev. D**84** 053013 (2011) [arXiv:1107.2308]
[57] Sarikas, S., Raffelt, G. G., Hudepohl, L. and Janka, H.-Th., Phys. Rev. Lett.**108** 061101 (2012) [arXiv:1109.3601]

[58] Sarikas, S., de Sousa Seixas, D.,& Raffelt, G., Phys. Rev. D**86** 125020 (2012)
[59] Saviano, N., Chakraborty, S., Fischer, T. and Mirizzi, A. Phys. Rev. D**85** 113002 (2012) [arXiv:1203.1484]
[60] K. Takahashi, K. Sato, H. E. Dalhed and J. R. Wilson, Astropart. Phys. **20** 189 (2003)
[61] Fogli, G.L., Lisi, E., Montanino, D. and Mirizzi, A., Phys. Rev. D**68** 033005 (2003) [arXiv:hep-ph/0304056]
[62] R. Tomas, M. Kachelriess, G. Raffelt, A. Dighe, H. T. Janka and L. Scheck, JCAP **0409** 015 (2004)
[63] S. Choubey, N. P. Harries and G. G. Ross, Phys. Rev. D**74** 053010 (2006)
[64] J. P. Kneller, G. C. McLaughlin and J. Brockman, Phys. Rev. D**77** 045023 (2008)
[65] J. Gava, J. Kneller, C. Volpe and G. C. McLaughlin, Phys. Rev. Lett.**103** 071101 (2009)
[66] Loreti, F. N. and Qian, Y.-Z. and Fuller, G. M. and Balantekin, A. B., Phys. Rev. D**52** 6664 (1995)
[67] G. Fogli, E. Lisi, A. Mirizzi and D. Montanino, JCAP **0606** 012 (2006) [arXiv:hep-ph/0603033]
[68] A. Friedland and A. Gruzinov, arXiv:astro-ph/0607244
[69] J. P. Kneller and C. Volpe, Phys. Rev. D**82**, 123004 (2010) [arXiv:1006.0913v2].
[70] J. P. Kneller, arXiv:1004.1288[hep-ph] (2010)
[71] Cherry, J. F., Wu, M.-R., Carlson, J., et al. Phys. Rev. D**84**, 105034 (2011)
[72] Kneller, J. P., & Mauney, A. W. 2013, [arXiv:1302.6601]
[73] Kneller, J. P., & Mauney, A. W. 2013, [arXiv:1302.3825]
[74] Borriello, E., Chakraborty, S., Mirizzi, A., Serpico, P. D., & Tamborra, I., Phys. Rev. D**86** 083004 (2012)
[75] Abe, K., Abgrall, N., Ajima, Y., et al., Phys. Rev. Lett.**107** 041801 (2011)
[76] Abe, Y., Aberle, C., Akiri, T., et al., Phys. Rev. Lett.**108** 131801 (2012)
[77] Ahn, J. K., Chebotaryov, S., Choi, J. H., et al., Phys. Rev. Lett.**108** 191802 (2012)
[78] An, F. P., Bai, J. Z., Balantekin, A. B., et al., Phys. Rev. Lett.**108** 171803 (2012)
[79] J. P. Kneller and G. C. McLaughlin, Phys. Rev. D**80**, 053002 (2009) [arXiv:0904.3823v1]
[80] Z. Maki M. Nakagawa and S. Sakata, Prog. Theor. Phys., **28** 870 (1962)
[81] K. Nakamura *et al.* [Particle Data Group Collaboration], J. Phys. G **G37**, 075021 (2010).
[82] P. Langacker, S. T. Petcov, G. Steigman, and S. Toshev, Nuclear Physics B, **282**, 589 (1987)
[83] A. Arcones, H. -T. Janka and L. Scheck, A&A **467** 1227 (2007) [astro-ph/0612582].
[84] C. A. Meakin and D. Arnett, Astrophys. J. **667**, 448 (2007) [astro-ph/0611315]
[85] P. R. Kramer, O. Kurbanmuradov, and K. Sabelfeld, Journal of Computational Physics **226** 897 (2007)
[86] C. Lunardini and I. Tamborra, JCAP **1207**, 012 (2012) [arXiv:1205.6292]
[87] B. Dasgupta, A. Dighe, A. Mirizzi and G. Raffelt, Phys. Rev. D **78**, 033014 (2008)
[88] M. Th. Keil, G. G. Raffelt and H.-Th. Janka, Astrophys. Jour. **590**, 971-991 (2003), [arXiv: astro-ph/0208035v2]
[89] T. Fischer, private communication, but data are based on [11].
[90] J. P. Kneller and G. C. McLaughlin, Phys. Rev. D **73**, 056003 (2006) [hep-ph/0509356]
[91] B. Dasgupta and A. Dighe, [arXiv:hep-ph/0510219]
[92] T. Lund and J. P. Kneller, *in preparation* (2013)